Elucidating the interplay of structure, dynamics, and function in the brain's neural networks

by

Sima Mofakham

A dissertation submitted in partial fulfillment
of the requirements for the degree of
Doctor of Philosophy
(Biophysics)
in The University of Michigan
2016

Doctoral Committee:

Professor Michal R. Zochowski, Chair

Assistant Professor Sara J. Aton

Associate Professor Victoria Booth

Professor Duncan G. Steel

Assistant Professor Qiong Yang

To Mohsen, my parents, and uncle Tony

ACKNOWLEDGEMENTS

I would like to thank my committee members for agreeing to serve on my dissertation committee and improved my dissertation by their comments and edits.

Thank you, Michal, for being such an amazing advisor, I have been incredibly fortunate to have you as my mentor. You taught me how to ask good questions, gave me insight on how to approach scientific questions and how simple ideas can solve the most complex problems. Besides all the science you taught me, during my graduate study you were such a kind and supportive mentor. I feel so much gratitude towards you that simply cannot be expressed in words.

Thank you, Victoria and Chris, I truly enjoyed working with you two on our collaborative project. Not only you are so knowledgeable and expert in the computational neuroscience field, but also, both of you have been so pleasant, accommodating and easy to work with. Chris, as a former labmate, you are my role model for being such a smart and at the same time humble person. Thank you, Victoria, for introducing me to famous people in the field. You always have been so kind to me, and treating me as one of your students.

Sara and Nicollet, your research is fascinating, and I enjoyed working with you. Thank you, Sara, you introduced a new horizon to me and gave me a taste of a real biology. It has been a blast working with you.

I want to thank my labmates Tony, Chris, Liz, Dan, James, Quinton and Jinxing for being such great friends to me. Dan, Tony, James, and Chris thank you for helping me to refine my programming skills; I learned a lot from each and every one of you. Liz thank you for being such a great friend, having you as a friend made me a better version of me. Dan, besides all the data analyzing you taught me, you were there for me whenever I needed help. James, you are a very caring and kind friend, plus your jokes are funny although I usually don't get them. Quinton and Jinxing we overlapped for a short period, but it was long enough to learn that you are such valuable additions to our lab.

Finally, I want to thank my parents and my sisters for their endless love and support. Last but not least, I want to thank my husband Mohsen, who have loved and supported me during this journey.

TABLE OF CONTENTS

LIST OF FIGURES

FIGURES

LIST OF ABREVIATIONS

AMD	Average Minimum Distance
CA1	Cornu Ammonis area 1
CFC	Contextual fear conditioning
CNO	Mice that administered the hM4Di ligand clozapine-N-oxide
DMSO	Vehicle-treated mice
FCA	Functional Clustering
FSM	Functional similarity matrix
GABA	Gamma-aminobutyric Acid
ISI	Interspike Interval
LIF	Leaky integrate-and-fire model
MPC	Mean Phase Coherence
PRC	Phase Response Curve
PV+	Parvalbumin-expressing interneurons
REM	Rapid Eye Movement Sleep
SWS	Slow Wave Sleep

CHAPTER I

Introduction

In ancient time, the heart was assumed to be the foundation of intelligence, emotions, and spirit. Today we know that the brain is in fact what makes each individual a unique "being" and losing a tiny fraction of this brain may have enormous effects on the individual memories, morals, and emotions. But what is this brain, how a physical foundation can be responsible for dreams and thoughts? How can this 1.5 kg mass can be accountable for Einstein's special relativity theory or Mozart's amazing pieces? How can it be Garry Kasparov and defeat the smartest computers of our times in a fair chess game? The answer is not easy, our knowledge about the world inside our brain is much less than the world around us. The underlying mechanisms of simple tasks such as face recognition are not clearly understood yet, much less on understanding the thought process, decision-making or consciousness. Our current understanding of the brain was founded in late 19th century. At that time, there was a huge controversy on the gray matter structure between Santiago Ramóny Cajal and Camillo Golgi. While, Cajal believed that the brain is made of individual cells, Golgi saw it as a continuous, diffused network of axons that couldn't be broken down to individual cells. Ironically, Cajal used the novel staining technique developed by Golgi and

showed that the brain is made of individual cells like any other organ. This revolutionary discovery transformed the field of neuroscience and brought Cajal and Golgi a shared Nobel prize in 1906 [1,2,3]. Today, we know that the brain consists of many different types of neurons with a wide range of structural characteristics and electrical properties. Despite all the differences neurons share a very similar job, which is to receive, integrate and transmit information [4]. Our interaction with world inside and around us is based on the opportune activity of these different kinds of neurons. This precise activity of neurons can be thought as a musical symphony where each and every function is encoded in a specific piece. But what is it that orchestrates this symphony? Physicists try to explain this emergence of large-scale patterns of neural activity by the similarity between the dynamics of a neuron and an oscillator [5]. Neural circuits could be modeled by a group of oscillators that are coupled together to coordinate different parts of the brain to perform diverse tasks. This, however, does not explain how these patterns of activity are translated to cognitive processes in the brain. The question remains how these neurons, slow units of information possessors (with an average firing rate of 15Hz greatly slower than any computer CPU), can result in this fast and efficient functioning brain.

To this date with all the technological advancements, especially in the field of computer science, still no computer can simulate all the brain activities even for a short period of time. The mystery behind this incredible performance has brought many physicists, mathematicians, computer experts and neuroscientist together to found a relatively new field of research known as Computational Neuroscience. Where computational techniques along with graph theory methods are used to create simple and realistic models of

individual cells and neural circuits of the brain [6]. In 1907 Louis Lapicaque introduced the integrate-and-fire model, first and the simplest mathematical model that mimics in a very basic way the changes in neuron's membrane potential [7,8]. It was until around 1952 that Hodgkin & Huxley's electrophysiological work on giant squid axon provided a very biological detailed model [9]. This model links macroscopic changes of ionic currents to the conductance of sodium and potassium channels and successfully explains generation and propagation of action potential. These models revolutionized the traditional field of neuroscience and shed light on how the function emerges from underlying neural networks.

In this chapter, I provide a brief introduction to the structure and function of neurons. I elucidate how the cell-to-cell interactions within these subunits form neural circuits. The underlying structure of these neural circuits is the key factor on shaping network dynamics and eventually the brain function. Unfortunately, our knowledge about the underlying structure of the brain is very limited. The undeniable dependency of the brain function on its structure attracted many scientists from diverse backgrounds to propose and optimize different models of neuronal connectivity. These proposed models are based on the anatomical evidence, the efficiency of information transmission and wiring cost. The brain structure, dynamics, and function are inseparable factors. Learning new skills could directly reflect on the physical structure of the brain, and, in turn, the brain structure could make it easier or harder to learn. The structure of the brain directly influences the formation of spatiotemporal patterns. These patterns on one hand determine the brain function while on the other they can adjust the structure through spike timing-dependent plasticity (STDP). Later, I discuss the formation of

different spatiotemporal patterns of activity, and how we can relate those to the function of the brain.

1.1 Neuron

1.1.1 Building block of the brain

The brain is a very complex network, made of hundred billion interconnected neurons [4,10]. Each of these neurons could be connected to as many as ten thousand other neurons. Thus, there are trillions of connections involved in forming the brain [11]. The brain structure is inseparable from its function; the specific way this complex network is connected shapes our mind, thoughts, talents, memories and personality. Thus, to have a firm grasp of the brain function, first we need to understand how its subunits are designed and work. Neurons are the smallest units of the information processor, which their particular physical and electrical design enables them to receive, process and communicate synaptic signals.

1.1.2 Neuron: structure and function

A typical neuron consists of three main parts: dendrites, cell body, and axon. Dendrites are the most distinctive parts of a neuron structure; one can classify neurons based on the shape of their dendritic tree. Dendrites are branched extensions projecting from the cell body and their main duty is to receive and transmit signals from surrounding cells to the neuron's cell body. The cell body or soma, contains the nucleus of the cell and produces

all the proteins needed for nerve cells' function. The incoming signals from dendrites are integrated at the cell body and if their summation is large enough it can generate an all-or-none electrical signal. This electrical signal is an action potential (AP) and it is generated at axon hillock, a specialized part of the cell body right before the axon. The axon is an elongated outgoing extension that transmits the generated action potential to the other cells, muscles, and glands. In human, axons may extend up to one meter, while their width does not exceed tens of micrometers. The giant squid axon that was used to study electrical properties of action potential was one-millimeter in diameter [12].

1.1.3 Neuron as an electrically excitable cell

Neurons hold an electrical potential difference across their membrane. This potential difference is called membrane potential and at rest has a typical value of -70mV [13]. The electrical activity of a neuron is linked to the fluctuation of the ions' concentration across its membrane. The membrane is a semipermeable barrier that selectively is more permeable to some ions, for instance, K^+ while others such as Na+ to transport across the membrane need special machinery. At rest, K^+ has a high cytosolic concentration and Na^+ holds a high extracellular concentration. This gradient of ion concentration is the driving force for generating an action potential.

Action potentials are all-or-none transient electrical events that make the cell-to-cell communication possible. The initial trigger of producing an action potential is receiving inputs from the other cells; these inputs are integrated at

the cell body and alter the membrane potential. The incoming perturbations may elevate the membrane potential and result in opening the voltage-gated Na^+ channels that are normally closed at rest (Voltage-gated channels are channels that their state is a function of the membrane potential). Upon the activation of sodium channels, Na^+ ions rush into the cell to diminish this concentration gradient. The elevated Na^+ concentration inside the cell, in turn, raises membrane potential even higher; if the membrane potential surpasses certain threshold it opens, even more, sodium channels that could result in a huge, transient upswing in the membrane potential known as an action potential (Fig. 1.1). Shortly after an action potential is triggered, voltage-gated potassium channels open to allow drift of interior K^+ ions to neuron's exterior. This efflux of K^+ ions shapes the falling part of membrane potential, that continues beyond the resting potential and hyperpolarize the membrane potential (Fig. 1.1). This hyperpolarization or the refractory period controls the maximum firing rate of neurons and last for a couple of milliseconds. Action potentials are generated at the axon hillock, where the membrane possessing the highest density of sodium channels. One can think of an action potential as a digital signal due to its all-or-none characteristics. Once action potentials are generated, it propagates through the axon toward axon's terminal. Axon terminal is a place enriched with neurotransmitters embedded in synaptic vesicles. These vesicles release their content in the synaptic cleft, a hundred nanometer gap between presynaptic and postsynaptic neuron, upon the activation of voltage-gated Ca^+ channels once action potential reaches the axon terminal [4].

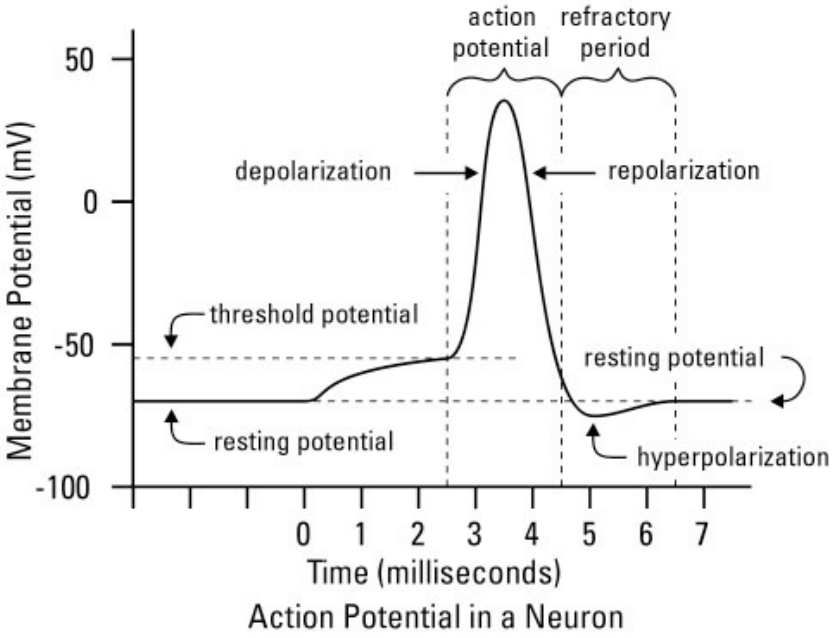

Figure 1.1 Illustration of different phases of a typical action potential. (Image is adapted from **https://psychlopedia.wikispaces.com/resting+potential** [14])

1.1.4 Synapse: As a bridge between digital and analog signal

Cell-to-cell communication of neurons occurs at specialized junctions, known as synapses. A synapse is a special structure where the axon terminal of presynaptic neuron comes in close proximity of postsynaptic dendrites (hundreds of nanometers). The arrival of an action potential at the axon terminal triggers the release of presynaptic neurotransmitters into the synaptic cleft, which consequently influences the state of receptors (being open versus closed) on the membrane of postsynaptic neurons. Depending on the type of released neurotransmitters, excitatory or inhibitory, the postsynaptic cell is injected with a positive or negative continuous current. Through chemical mediums, synapses convert digital signals (all-or-none action potentials in the presynaptic neurons) to analog signals (continuous signals) depolarizing or hyperpolarizing the postsynaptic cell.

1.1.5 Neuromodulation controls activity of a large population of neurons

Synapses allow neurons to directly influence each other's activity, although interactions among neurons are not limited to cell-to-cell interactions. Neurons can control each other's activity indirectly through neuromodulation. Neuromodulation is a mechanism where specific cells release certain chemicals (neuromodulators) in the extracellular space and through which regulate the activity of a diverse population of neurons. Acetylcholine, dopamine, norepinephrine, and serotonin are the most studied neuromodulators; they can diffuse to a large area of nervous system and regulate the brain dynamics. Specifically, Acetylcholine is a neuromodulator that controls neurons excitability, its has been shown that it's in high concentration during wake and absent at sleep [15,16,17,18]. Dopamine is another neuromodulator that controls the reward-motivated behavior and motor control [19,20]. For example, Parkinson's disease and depression are linked to the deficiency of dopamine, and their treatments involve specifically designed drugs to increase the dopamine level [21, 22].

1.1.6 Classification of Neurons

Neurons are similar in their function, which is to receive, process and transmit information via electrochemical signals; however, each neuron can be quite unique. Neurons can be classified based on (a) their direction of information transformation (afferent: travels from tissue to the brain; efferent: travels from the brain to tissues), (b) the effect they have on the

target neuron (excitatory or inhibitory), (c) neuron's anatomical appearance (pyramidal: triangular soma, stellate: star-shaped dendrite tree, granule: small and round cell body), (d) or spiking patterns, (e) neuron's structure (unipolar, bipolar or multi-polar) [4] and finally (f) based on their excitability profile. Neuronal excitability falls into one of two broad categories, depending on the bifurcation structure observed in the neuron's transition to firing. In Type I neurons, repetitive spiking is initiated by a saddle-node on an invariant cycle (SNIC) bifurcation. These neurons act as integrators, with firing frequency increasing sharply from the arbitrarily low levels observed at firing threshold, and they exhibit a low propensity for synchrony when coupled by excitation. Type II neurons transition to firing through an Andronov-Hopf bifurcation, leading to a discontinuous and shallow frequency-current curve, and higher propensity for synchronization when coupled together [23,24].

Generally, these excitability types result in different profiles of the neuronal phase response curves (refer to chapter II for details of computing PRC), which capture the neuronal response to brief stimulation [25,26,27]. Type I cells exhibit exclusively phase advances in response to stimuli arriving at different times during the firing cycle, while Type II cells display both phase delays and advances. Experimental results show that both of these cell types are present in the brain, with some neurons capable of switching types [28].

1.1.7 Neuron as a simple RC circuit

A cell membrane consists of phospholipid bilayers that separate intracellular and extracellular ions and transmembrane proteins (ion pumps and channels)

that regulate the passage of these ions across the membrane. Phospholipids are amphipathic molecules owning hydrophobic tail and a hydrophilic head. For the sake of minimizing structural energy consumption, they adopt a thin lipid bilayer where they hide the hydrophobic tail inside and sticking out the hydrophilic head. This arrangement results in an insulator layer, separating intracellular and extracellular charges across the membrane. Transportation of essential ions for nerve activity, across this lipid bilayer, is only possible via the specialized ion channels and pumps embedded in the membrane. This specific structure of the membrane enables neurons to function as timely and accurate as needed.

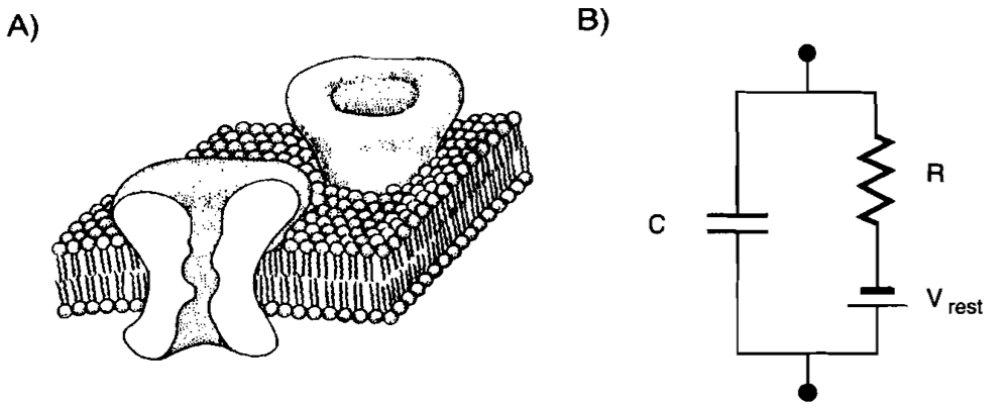

Figure 1.2 Modeling a cell membrane using an RC circuit. (Image is adapted from [13])

To mimic the electrical activity of a neuron, one can model neuron's cell membrane by replacing its insulator lipid bilayer with a capacitor and its ions channels and pumps that actively control the passage of ions across the cell membrane with a resistor in a parallel fashion with the capacitor (Fig. 1.2). In an RC circuit if you inject current somewhere between resistor and capacitor, based on Kirchhoff law it splits into two parts while the sum

remains the same. A portion of this current departs to the resistor side (I_R) and leaks while the remaining current set out to charge the capacitor (I_C).

$$I_{drive}=I_R + I_C \quad (1.1)$$

The relationship between charge and voltage across a capacitor is as follow:

$$Q= CV_m \quad (1.2)$$

where Q is the separated charge across the capacitor and C is the capacity. We can rewrite equation 1.1 by substituting I_C with derivative of equation (1.2) and I_R from Ohm's law as follow:

$$I_{drive} = C\frac{dV}{dt} + \frac{V}{R} \quad (1.3)$$

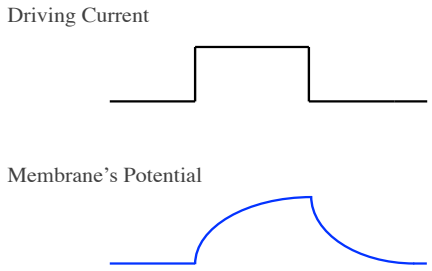

Figure 1.3 Membrane potential as a function of driving currents. Injecting positive current inside the cell, increases the voltage across the membrane in an exponential fashion and ceasing this current results in the exponential decay of this potential.

This simple linear one-dimensional partial equation can capture the changes in the electrical potential across the membrane as a function of driving current. By assuming the initial condition of $V_{(t=0)}=0$, the general solution for equation (1.3) is:

$$V = IR(1 - e^{-\frac{t}{RC}}) \quad (1.4)$$

Where the RC is the time constant of the membrane, normally denoted with 'τ_M' and shows how fast the exponential function changes with time. Relatively a long time after injecting the current, V reaches the steady state where V (t=∞) equals to IR and the RC circuit behaves like a resistor (Fig. 1.3a). Membrane's time constant reflects on the pace of evolving membranes' voltage in response to the driving current. When 'τ_M' is so short, changes on the membrane's voltage is quick and manipulated by varying adjacent temporal events but when 'τ_M' is long it's affected by the events happened while ago and develops some kind of memory (Fig. 1.3b). By ceasing the driving current the voltage decreases, again in an exponential fashion with τ_M, as below:

$$V = IRe^{-\frac{t}{RC}} \quad (1.5)$$

Here an external source is used to provide the injected current; in the brain, these driving current are due to the excitatory (positive driving current), and inhibitory (negative driving current) synaptic inputs. So we can replace the driving current with a battery (representing the resting potential of synaptic ion channel E_{syn}) and a resistor with the conductance of $g_{syn}=1/R$ (for incoming synaptic currents) in parallel to the existing RC circuit (Fig. 1.4). In this case, we can rewrite equation 1.4, and for the sake of simplicity we replace R (resistance) with g (conductance) as follow:

$$V = \frac{(g_r E_r + g_s E_s)}{g_r + g_s}\left(1 - e^{-\frac{t(g_r+g_s)}{c}}\right) \qquad (1.6)$$

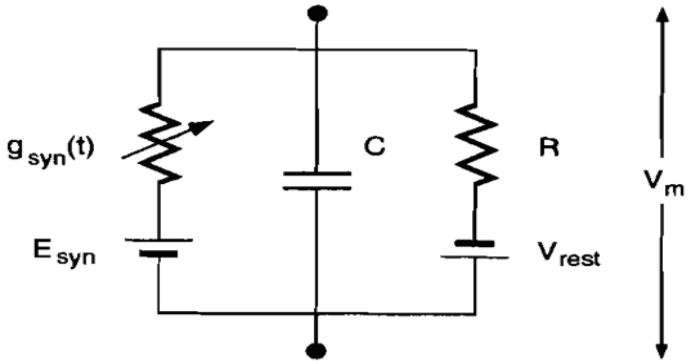

Figure 1.4 RC circuit when driving current comes from a fast chemical synapse.
(Image is adapted from [13])

1.2 Neural networks in the brain

1.2.1 Neural Circuits

The brain is the most complex self-organized biological system. It is made of hundred billion neurons and each of these neurons can synapse to up to 10000 other neurons [11]. The brain's function as any other self-organized system cannot be solely encapsulated by its individual constituting units, but also, it's highly affected by the way these units interact to each other [30,31]. Thus, to gain insight into the brain function, we need to study the brain in the context of neural ensembles or neural circuits.

1.2.2 Network connectivity

The incredible performance of the brain is made possible via the interactions of neurons in neural networks [32,33]. These interactions are mediated through

physical connections as well as dynamical properties on the interconnected cells. After many years of research started with Santiago Ramón Cajal drawings, until today with all the advanced techniques and parallel projects on mapping the brain (BRAIN initiative project [34], human connectome project [35], and clarity project [36],...) we still lack a well-defined brain connectivity map.

When it comes to the brain connectivity paradigm, one can define two different connectivity paradigms: anatomical, and functional connectivity. Anatomical connectivity describes the existing physical connections in the brain. If it's not impossible, it will be extremely hard to obtain a comprehensive anatomical structure of the brain. It requires tracking hundred billions of neurons and each and every axon and dendrite radiating from their cell bodies. Even if we could acquire such a physical map, it's not capable of delivering a realistic representation of the brains' connectivity pattern. How do we know which synapses are active or silent? Or how strong is each synapse? Even if we freeze the time and know all the synapses and their associated synaptic efficacy at one point of time, the brain function is entangled with constant change and plasticity that constantly form new synapses or modifies the synaptic efficacies of existing synapses [32].

Functional connectivity, on the other hand, captures the functional dependencies of neurons to one another based on the statistics of their firing patterns. Relatively new imaging techniques such as functional magnetic resonance imaging (fMRI) [37,38] or electrophysiological recordings techniques such as electroencephalogram (EEG) [39,40] has made some progress in revealing the functional connectivity of the neuronal ensembles, but still lack enough resolution to detect single neuron activity [37].

1.2.3 Analysis of network connectivity

To shed light on the basis of the brain function, scientists employed graph theory to create a connectivity model that closely fits the anatomical and functional necessities of the brain's connectivity [41]. In graph theory, networks are built by using a group of 'nodes' (representing neurons) that are connected to each other via links called 'edges' (synapses), the way these edges are distributed among nodes shapes the structure and consequently function of each particular network. Among many different models suggested for the network structure from all-to-all connectivity to sparse random connectivity, some models are more realistic due to their low-energy cost, high speed of information transmission, and meeting anatomical needs.

1.2.4 Optimizing network connectivity: Small world paradigm

What is an optimal network design which brain could utilize? To answer this question we need to consider two important factors, wiring cost and efficient global information transfer. The wiring cost of the brain scales with the connection length, and favors local connections. This can be a driving force in the formation of distinguished functionally specialized neuronal assemblies across the cortex such as the primary visual system and somatosensory cortex. The primary connectivity profile in these areas are cortical-cortical, they are heavily locally connected and often connections are reciprocal-providing feed-forward and feed-back loops [42].

On the other hand, an efficient information transfer is an indispensable factor. The human brain is a very complex biological structure with a long synaptic distance (steps) between the initial sensation, cognition, and action. This long synaptic distance (steps) integrate information from different parts of the brain, therefore, a fast coordination of these regions are vital for a proper functioning brain. This quick coordination is only possible through long-distance connections among these specialized regions. Previous studies on the connectivity of prefrontal, lateral temporal and limbic system identifies hubs connecting long-distance areas [43]. In fact, the ratio of the number of long-distance connections to local connections is an indicator of evolution in cognitive functions such as language and reasoning [44]. Taken these observations together, a proper model of the brain connectivity should be a combination of mostly local connections along with some long-distance connections.

Small-world connectivity is one of the most appealing connectivity models due to its high clustering coefficient, short average path-length and low wiring cost [45]. In this model network is comprised of mostly local and some random connections, which of its own accord suitably matches our gross knowledge of connectivity within the cortical columns [46,47,48]. In this paradigm, we originally connect every neuron to its nearest neighbors in a radius of 'R', and then by defining a rewiring probability (P), we allow some of these connections to break and form a new connection to a randomly chosen neuron. This model provides an easy framework to interpolate between a locally connected network and a completely random network by changing rewiring probability (Fig. 1.5).

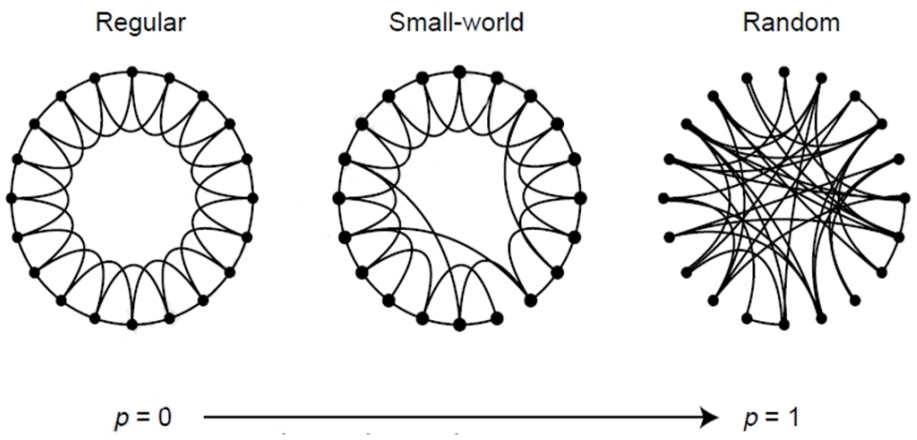

Figure 1.5 Schematic illustration of small-world connectivity paradigm. Depending on the defined rewiring probability, network structure could vary between a regular, lattice-like network and a random network. **(**Image is adapted from [45])

1.2.5 Scale free and Rich Club connectivity

Scale free connectivity paradigm is another attractive model to simulate the brain connectivity. Scale free model gained its fame after Albert-László Barabási study on the worldwide web structure, showing that the number of edges per nodes follows a power law distribution [49] as follow:

$$P(k) \sim k^{-\gamma} \qquad (1.7)$$

Where P(k) is the fraction of neurons with k connections to the rest of the neurons. In this structure while the most of the neurons are sparsely connected, there are few neurons that are highly connected to the rest of the network (Fig. 1.6b). These neurons are called hubs and later many studies on the brain speculated on their role on coordinating different parts of the brain for cognitive tasks [49, 50,51].

The rich-club is an interesting structure, in which aforementioned hubs found

a higher order structure by making many connections to the other hubs (Fig. 1.6c). The brain has a tendency to minimize its wiring cost (proportional to the length of connections) both in cellular scale and mesoscale among functionally specialized regions. The particular structure of rich-club provides a low wiring cost and nicely fits the economic needs of brain [52,53,54,55,56].

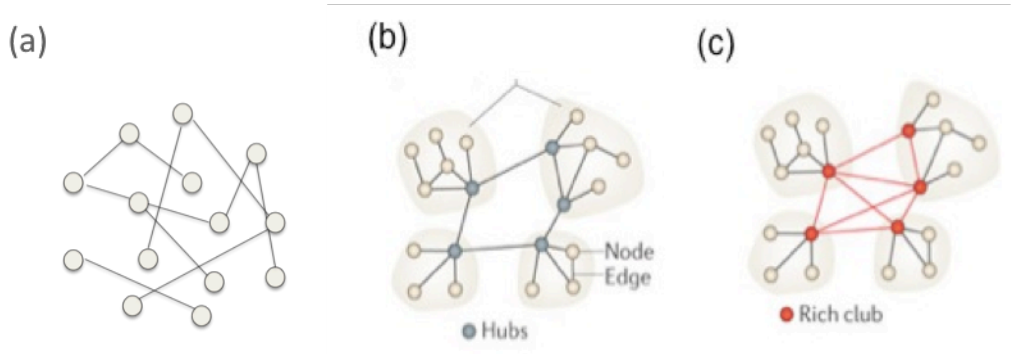

Figure 1.6 Schematic representation of random, scale free and rich-club connectivity paradigms. a) Sparse random connectivity, b) scale-free connectivity includes few neurons that are richly connected to the rest of the network, while most of the neurons are sparsely connected. c) Rich-club is a higher order structure made of interconnecting hubs. (Image is adapted from [57])

1.3 Spatiotemporal patterning

Thanks to Hodgkin-Huxley [9] work on squid giant axon, today we have a clear understanding of an individual neuron's dynamics. Simply, each neuron has two distinct dynamical states: quiescent or spiking, which can be explained based on Hodgkin-Huxley equations. Not only the activity state of neurons, spiking versus quiet is important, but also the temporal patterns of each neuron's spike times contains hidden information that neuron commute

to the rest of the network. The key to understanding how the brain works is in decoding these spike times.

1.3.1 Frequency coding versus temporal coding

Neurons are simple units of information processors; they encode information and commute it to the rest of the network with spiking. But the question is how they encode information and how to retrieve this encoded information from spiking patterns? One can look at spike times in two distinct ways: a) frequency or rate coding and b) temporal coding. Frequency or rate coding is the simplest way to speculate about a stimulus. This scheme only considers the average firing frequency of a neuron, where the intensity of the stimulus is directly proportional to the firing frequency. Despite the over simplicity involved in this scheme, it has been exhibited some success in the case of particular nerve cells. For instance, the electrical activity of sensory neurons appears to be directly influenced by the strength of the stimulus [4]. However, generally speaking, the brain diverse functions are too complicated to be only coded with the firing rate. Imagine you have two different time series; one looks like 0000011 and the other 1000001. Although, these time series share the same average firing rate but they could carry complete different information. Therefore, many neuroscientists believe that to decode neurons time series, one need to consider temporal patterns and the precise timings of spikes [58,59].

1.3.2 Brain from physicists' point of view

The complexity and mystery involved in the astonishing performance of the brain made it very attractive to the curious mind of a physicist. We, as physicists, understand complex systems such as the brain, by breaking it down to simplifying entities that can be explained by fundamental laws of physics. Having said that, we see the building blocks of the brain these detailed biological units nothing more than simple oscillators that are coupled together to coordinate and synchronize different parts of the brain for different tasks. As G*yörgy Buzsáki* wrote in his *Rhythms of the Brain* book "*This feature (synchrony) is built into their (oscillators) nature. In fact, oscillators do not do much else. They synchronize and predict. Yet, take away these features, and our brains will no longer work. Compromise them, and we will be treated for epilepsy, Parkinson's disease, sleep disorders, and other rhythm-based cognitive maladies* " [5].

Oscillatory behavior can be seen in neuron's individual activity such as membrane potential oscillations [60] or in the rhythmic firing patterns of neuronal network that produce different cortical rhythms in frequencies different than individual cells' frequency [61]. In many cases, these oscillations are the key for the certain brain's function [62,63,64]. There is a vast body of research devoted to the relationship of these rhythms and certain functions, examples of which are gamma rhythms recognized for its involvement in cognitive functions such as attention [65,66] and visual perception [67,68,69,70] or theta rhythms associated with memory formation and consolidation [71,72,73].

1.3.3 Synchrony in the brain

The brain accomplishes different cognitive tasks, by integrating and coordinating enormous amount of information coming from different specialized functional regions. Previous studies debated that these super fast coordination is mediated via some transiently synchronized activity of functionally related neurons [74,75]. But, what do we mean by synchronized activity of neural network? The synchronized activity of neurons can be defined by the simultaneous firing of a group neurons followed by a silence period [5]. Hans Berger first detected the existence of the synchronous patterns of activity in 1929, after several years recording electrical activities of the brain in hopes of finding any scientific evidence that can prove/explain telepathy. Although he never proved electromagnetic transmission from one brain to another, he discovered brain rhythms in his recordings [5]. Today we know of many brains rhythms and different roles that they play in the brain cognitive functions [5].

1.3.4 In-phase versus out-of-phase synchrony

There are different kinds of synchrony in the brain: a) In-phase synchrony or complete synchrony: all the neurons start and finish their cycles together, b) Out of phase synchrony: oscillators are synchronized by a certain phase lag that is maintained unchanged over time. For out of phase synchrony, one can think of two pendulums when the first one is at the maximum the second one is always at the minimum, and they constantly maintain a certain phase lag ($\pi/2$) throughout their activity. Technically these pendulums are phase-lock

to the same rhythm. Phase-locking is a more general form of synchrony, and could have a significant role in different brain's functions. An example of which can be seen in hippocampal memory formation, where phase-locking to theta rhythm is essential for memory formation and consolidation [76].

1.3.5 Synchrony in a pathological brain

In spite of the great role of synchrony in diverse higher order cognitive functions, many neurological disorders such as epilepsy, Parkinson's disease, Alzheimer, and Schizophrenia have also been correlated to the abnormal synchrony [77]. In Parkinson's disease, thalamic neurons exhibit abnormal synchronous activity that disrupts the temporal coding of motor related activities and causes tremor and movement difficulties [78]. Epilepsy is another neurological disorder, linked to the excessive synchronous activity of neural networks [79]. Any brain under specific circumstances such as severe sleep deprivation or structural changes (as might happen after a head injury or tumor) can experience seizures. However, in the case of epilepsy patients, seizure starts exclusive of any physical indication, it just happens as the epileptic brain bears some alternations. EEG recordings from patients with epileptic seizures reflect a low amplitude high frequency during the pre-ictal period followed by high amplitude signals throughout the ictal period (Fig. 1.7) [80]. Previous studies have shown that this high amplitude recorded activity during the ictal period are not only hyperexcitable states due to the imbalanced interaction of excitatory-inhibitory neurons but also they are closely related to the enhanced degree of synchrony in neuronal circuits [77,81,82].

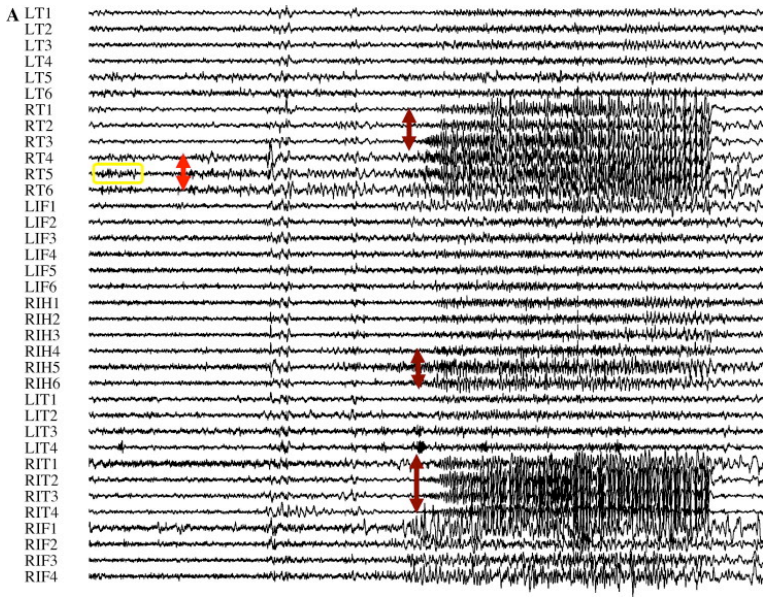

Figure 1.7 EEG recordings from a patient with epilepsy. One can see high-frequency pre-ictal oscillations followed with high amplitude oscillations corresponding to seizure onset. **(**Image is adapted from [83])

1.3.6 Understanding interaction between structure and dynamics in neural networks

Brain structure, dynamics, and function are deeply intertwined. To understand how brain functions, it is crucial to uncover the links between network structure and its dynamics. To identify the link between structure and dynamics we take two different approaches. In the first approach we model simpler neural network that could potentially represent a part of the brain, then we study how this structure is linked to dynamics. We employ this approach in Chapter II and III of this dissertation. A simple example of which is in Chapter III where we change network structure by interpolating rewiring

probability, which results in diverse range of dynamics from delayed propagating waves of activity to complete synchronous network activity [84].

The second approach is to start with the experimentally recorded time series and try to decode and quantify dynamics. Ultimately we aim to link the dynamical changes to the brain function and speculate on the possible structural changes. To decode spike times we need to develop measures to detect statistically significant correlations. Ideally, such measures extract statistical significance of spatiotemporal correlations and identify emergent patterns in the dynamics to provide network's functional connectivity. Such functional connectivity can be very beneficial to detect structural changes upon specific cognitive functions, for example, testing formation of new memories and their consolidation by creating new synapses [85,86]. Where if a memory is formed in neuronal circuit, the consequence of strengthening some synapses and weakening others can manifest itself through increasing the functional connectivity of neurons involved in shaping the memory and decreasing functional connectivity of the others [32]. Carla Shatz summarized the Hebbian learning theory as " Cells that wire together fire together" [87]. Thus, the spike timings of functionally connected neurons, involved in the new experience/memory will have a close temporal correlation. Based on the changes on the functional connectivity we could deduce possible functional and structural changes. An example of this approach is in chapter IV, where we examine memory consolidation by assessing the stability of network-wide functional connectivity over time.

1.4 Outline

The overall aim of this dissertation is to uncover some of the links between the network structure and its dynamics, to obtain a novel insight on how the brain functions. We explore key factors influencing the network structure, dynamics, and eventually function.

In chapter II, I investigate how the interplay of cellular properties with network coupling characteristics could lead network dynamics toward synchronous or asynchronous dynamics. More specifically, I identify conditions that promote synchrony in mixed networks of Type I and Type II neurons under varying network connectivity topologies. We show that for similar network structures, network synchrony may change significantly depending on the distribution of a number of shortcuts among Type I, and Type II neurons. This result is robust with changing heterogeneity, rewiring probability, synaptic efficacy and different fractions of Type I and Type II neurons.

To examine this effect further, for a loosely connected mixed network of Type I and Type II neurons with completely asynchronous dynamics, we create cliques by interconnecting few Type I or Type II neurons. We show if this clique is made of highly rewired neurons with Type II excitability, network has a high chance of adopting synchronous activity, however, the same clique of Type I highly rewired cells does not improve synchrony.

These results can be of high significance in respect to sleep/wake modulation of neuronal excitability in the brain. It was shown that intrinsic excitability of neurons can be modulated by acetylcholine levels in the brain. We show that relatively few neurons expressing receptor that are sensitive to

the Ach levels can dramatically change network-wide dynamics. Also, the synchronizing role of Type II cliques may be also important for the pathological brain function. It has been shown that upon an injury in the dentate gyrus, its circuits undergo architectural rearrangement including the formation of new connections among excitatory granule cells. These changes make its circuit hyperexcitable and prone to seizure. We show that if there are such rearrangements that create cliques of Type II excitability, these cliques have the potential to drive the networks dynamics to a highly synchronous state. *This chapter was submitted for publication in January 2016.*

Understanding spontaneous transitions from asynchronous to synchronous dynamics is vital since they may separate pathological and normal functions of the brain. In chapter III, I develop a set of measures that quantifies and predict these autonomous network transitions from asynchronous to synchronous dynamics under various conditions. The developed measures are potentially very interesting since it can be calculated in real time and therefore potentially applied in clinical situations. *This chapter was published in PLOS ONE journal in 2015* [88].

Chapter IV of this dissertation is devoted to the analysis of mice brain activity experimentally recorded in Aton's laboratory. In this chapter, we try to extract dynamical underpinnings of learning and memory consolidation from recorded spike times. Our laboratory has developed a set of tools capable of drawing underlying functional connectivity of network by extracting statistically significant temporal correlates of spike timings. I employ these tools and later compute the stability of the obtained functional connectivity over time, and compare this to behavioral tests for learning and

memory consolidation. We observed that stability is a good predictor of memory consolidation. I further applied these analytical methods to characterize the importance of network-wide oscillations to mediate stability and memory consolidation and showed that reduction of theta power oscillations leads to decrease in network stability. *This chapter is part of a manuscript that was submitted for publication in October 2015* [89]

CHAPTER II

Interplay between excitability type and neuronal connectivity in determining neuronal network synchronization

The interplay between neuronal excitability properties and global properties of network topology is known to affect network propensity for synchronization. Here, we identify conditions that promote synchrony in mixed networks composed of neurons having Type I and/or Type II Phase Response curves, and having varying connectivity statistics. Namely, we study small-world networks with fixed network-wide properties, but allow neurons to vary the number of re-wired connections they project. We show that even if the global connectivity properties of the network are the same, network synchrony may change significantly depending on the distribution of the number of re-wired connections among Type I and Type II neurons. We also show that establishing higher-order clusters by linking cells with the highest number of re-wired connections may elicit synchronous activity, depending on the excitability type of these neurons. *The work presented in this chapter was submitted for publication to journal of Physical Review E (PRE), and it was performed in collaboration with Victoria Booth, Christian*

G. Fink, and Michal Zochowski. I performed all the simulations presented here, and I was involved in the overall design of the project.

2.1 Introduction

Synchronization of neuronal networks has been associated with many brain functions, including attention and memory formation [90,91,92,76]. Aberrant synchrony is implicated in many pathologies of the brain, such as epilepsy [81], Parkinson's disease [93,94] and schizophrenia [95], underscoring the need to better understand mechanisms generating synchronization of neuronal networks.

The emergence of synchronous spatiotemporal patterns may be explained by two broad classes of mechanisms: 1) excitability properties of individual cells, and 2) characteristics of network coupling. As it was mentioned in the introduction, neurons can be classified based on the bifurcation structure observed in the neuron's transition to firing. Type I neurons can be identified with high excitability and little tendency for synchrony when they are coupled to other excitatory neurons. While Type II neurons are known for low excitability and high propensity to synchronize their spikes with other coupled excitatory neurons.

Different frameworks for network connectivity have been used to investigate the influence of network topology upon neuronal synchronization [47]. Among these models small-world model and scale free architecture are particularly appealing. The small-world model features high clustering coefficient and small path length. This model uses a single parameter, the rewiring

probability, to interpolate between a locally connected network and a completely random network [96]. The scale free architecture introduces richly interconnected neurons called hub cells, which have been shown to orchestrate synchrony in experimental models of epilepsy [49,51,50]. The derivative of the later is the "rich club" structure [53,52,56,54,55] characterized by highly interconnected hubs. Previous work has shown that correlations between neuronal excitability type and network structure dramatically influence network synchrony [24].Recently we showed, for instance, synchronize much more readily when hub cells are Type II excitability, rather than Type I [97].

In this chapter we investigate the effect of correlations between excitability type and connectivity structure in a network that is composed of neurons having varying connectivity properties with other cells. Specifically, we use small-world network models with different nodal distributions of re-wired connections to determine the effect of correlations between neuronal excitability type and the number of out-going re-wired connections. We show that long-tailed distributions, such as the exponential distribution, may have higher propensity for synchronization, indicating that few highly re-wired cells might drive synchrony in a network as a whole. Furthermore, the networks in which Type II cells have a large number of re-wired connections synchronize much better than networks in which Type I cells are highly re-wired. We also investigate the effect of forming clusters among the highly re-wired cells and show that interconnecting the most highly re-wired cells enhances synchronous dynamics when such cells are Type II, but not when they are Type I.

2.2 Methods

2.2.1 Phase Response Curve

We use the phase response curve (PRC) to identify excitability properties of the neurons. It is a metric that characterizes the influence of a perturbation, upon the trajectory of an oscillator. The PRC of an individual neuron, measures the shift in spike timing due to a single synaptic input:

$$\Delta(\theta)=\frac{T_{original}-T_{Perturbed}(\theta)}{T_{original}} \quad (2.1)$$

where θ is the phase at which the input is received, $T_{original}$ is the period of the unperturbed oscillator, $T_{perturbed}$ is the duration of the spike cycle during which the input is received, and Δ can be positive (phase advance) or negative (phase delay).

Neurons are classified based on their PRC properties (Fig. 1b): Type I PRCs feature phase advances regardless of the perturbation phase, while Type II PRCs are biphasic, showing phase delays for early synaptic input and phase advances for late synaptic input. The biphasic PRCs of Type II neurons provides them in some sense with more flexible spike timing control than Type I neurons, leading to enhanced propensity for synchronization in excitatory networks [25,26,27].

2.2.2 Cortical Neuron Model

We employed a Hodgkin Huxley type neuronal model with a fast inward Na^+ current, delayed rectifier K^+ current, and a leakage current. Cholinergic modulation has been experimentally shown to switch cortical neurons from

Type II to Type I PRC [28], and we model this effect with a slow, low threshold K^+ current (gated by g_{Ks}) responsible for spike frequency adaptation. Decreasing g_{Ks} from 0.8 mS/cm^2 to 0.1 mS/cm^2 mimics the effect of ACh in switching neuronal PRC from Type II to Type I [98]. Therefore equation governing neuronal dynamics is given by:

$$C\frac{dV_i}{dt} = -g_{Na}m_\infty^3(V_i)h(V_i - V_{Na}) - g_{Kdr}n^4\,(V_i - V_K) - g_{Ks}s(V_i - V_K)$$

$$-g_L(V_i - V_L) + I^{drive} + I^{syn}\,, \qquad (2.2)$$

where C =1.0μF/cm^2 and I_i^{syn} is the synaptic current. The synaptic current from neuron 'j' to 'i' is governed by:

$$I_{ij}^{syn} = W\exp\left(-\frac{t-t_j}{\tau}\right)(V_i - E_{syn}), \qquad (2.3)$$

t_j is the spike time of neuron j, and W is the synaptic strength which was kept constant for all the connections, and we fixed τ=0.5 ms and E_{syn}=0 mV. I^{drive} is an externally applied current that remains constant for each neuron within a simulation, but depending on the heterogeneity level needed for each simulation the spread of external current across neurons was set appropriately. In all the simulations in this chapter, I^{drive} was set to generate

average of 15 Hz with frequency spread of 26.6%, Type I: $I^{drive} = 0.158 \pm 0.038$, Type II: $I^{drive} = 1.22 \pm 0.18$. This frequency spread kept the same for all the simulations except those associated with figure 2.5, where the frequency spread changes from 0% (0Hz) to 52% (8Hz), Type I: $I^{drive} = 0.158 \pm 0.076$; Type II: $I^{drive} = 1.22 \pm 0.37$. The value of constant parameters used in this model are the same for both Type I and Type II neurons except

g_{Ks} which is g_{Ks}=0.1 for type I and g_{Ks}=0.8 for Type II neurons: g_{Na} = 24.0 ms/cm^2, g_{Kdr} = 3.0 ms/cm^2, g_L = 0.02 ms/cm^2, V_{Na} = 55.0 mV, V_K = −90.0 mV, and V_L = −60.0 mV.

In equation (2.2) m_∞ and h are responsible for activation and inactivation of Na current, and their dynamics are governed by $m_\infty(V) = 1/(1 + e^{(-V - 30.0)/9.5})$ and $dh/dt = \alpha_h(h_\infty(V) - h)/\tau_h(V)$,with $h_\infty(V) = 1/(1 + e^{(V + 53.0)/7.0})$ and $\tau_h(V) = 0.37 + 2.78/(1 + e^{(V+40.5)/6.0})$.The dynamics of the gating variable for the delayed rectifier potassium current were given by $dn/dt = (n_\infty(V) - h)/\tau_n(V)$, with $n_\infty(V) = 1/(1 + e^{(-V - 30.0)/10.0})$ and $\tau_n(V) = 0.37+ 1.85/(1 + e^{(V +27.0)/15.0})$. Finally, the gating variable for the slow, low threshold potassium current was governed by $ds/dt = \alpha_s (s_\infty(V) - s)/75.0$, and $s_\infty(V) = 1/(1 + e^{(-V - 39.0)/5.0})$.

2.2.3 Network Structure

We model networks of 1000 excitatory cortical pyramidal cells with 4% connectivity (40 outgoing connections per neuron), situated in a one-dimensional ring with periodic boundary conditions. The Watts-Strogatz small-world network is a popular paradigm for generating network connectivity, with R specifying the initial radius of local, lattice-like connectivity and P specifying the probability of each connection being rewired to a randomly chosen neuron.

Here we modify Watts–Strogatz‘s Small-world approach by first specifying the mean rewiring probability (P), and consequently total number of rewired connections in the entire network, then employ a specified distribution to assign the number of rewired connections projecting from individual

neurons. We used three different distributions: a) "No Variance" connectivity, in which all neurons shared the same number of rewired connections. With p=0.15, for example, every neuron has exactly 6 out of 40 outgoing connections randomly rewired. b) Uniform distribution with a defined average and fixed variance. For p=0.15, the average number of rewired connection per neuron was 6, with a range of ± 4 rewired connections c) Exponentially decaying distribution with a mean of 6. We compare these connectivity paradigms with conventional small-world topology, which features Poisson distribution.

2.2.4 Synchrony Measure

The Golomb synchrony measure was used to quantify network synchronization [99,100]. This is a simple measure based on computing the mean population-averaged fluctuations over an extended period of time, normalized to the average of individual neurons' fluctuations. In order to calculate the synchrony index (λ) from spike timings, they were convolved with a Gaussian (2ms width), averaged across all neurons at each time point, and the variance across time was computed (σ_V^2). The variances of individual neuronal voltage traces across time were computed, and then averaged over all neurons(σ_{Vi}^2). λ was then computed as:

$$\lambda = \sqrt{\frac{\sigma_V^2}{\frac{1}{N}\sum_{i=1}^{N}\sigma_{V_i}^2}} \tag{2.4}$$

λ is bounded between 0 and 1, zero for asynchronous dynamics and 1 for complete synchrony across the network.

2.3 Results

The aim of this chapter is to investigate, in mixed networks of excitatory Type I and Type II neurons, how various distributions of individual neuronal synaptic connectivity characteristics affect overall network dynamics. Neurons with Type I PRC exhibit purely positive phase shift and respond to small perturbations by advancing their phase, regardless of perturbation phase. Type II PRC neurons response to perturbation highly depends on the timing of the perturbation; if perturbation happens too early in the cycle it delays the next spike and if it happens later in the cycle it advances the next spike. Furthermore, Type I neurons are highly excitable, with low firing threshold and steep slope for their frequency-current (F-I) curve. Type II neurons, on the other hand, exhibit shallower F-I curve with high frequency threshold (figure 2.1a,b). We employed a modified version of Hodgkin Huxley to model these different types of excitability, where the conductance of a slow potassium current determined the excitability type [98].

2.3.1 Network structure in respect to the excitability types

Our connectivity paradigm extends the standard small-world protocol [96] to consider different local distributions of re-wired connections, given a fixed total number of re-wired connections throughout the entire network. In the standard small-world connectivity paradigm, each synaptic connection is assigned the same re-wiring probability, which determines whether its target will remain a neighboring cell or be re-wired to a random target cell in the network (independent of their distance). This paradigm results in an approximately Poisson distribution for the number of re-wired outgoing connections per neuron (Fig. 2.1c top). In our modified network

connectivity framework, we construct uniform and exponential distributions for the number of re-wired connections per neuron, as well as no variance (where all neurons share the same number of re-wired connections) in the distribution.

In these frameworks, instead of assigning a constant rewiring probability for each connection, each neuron is randomly assigned the number of outgoing re-wired connections it projects. These random assignments are drawn from one of the aforementioned distributions, with all distributions sharing the same total number of re-wired connections.

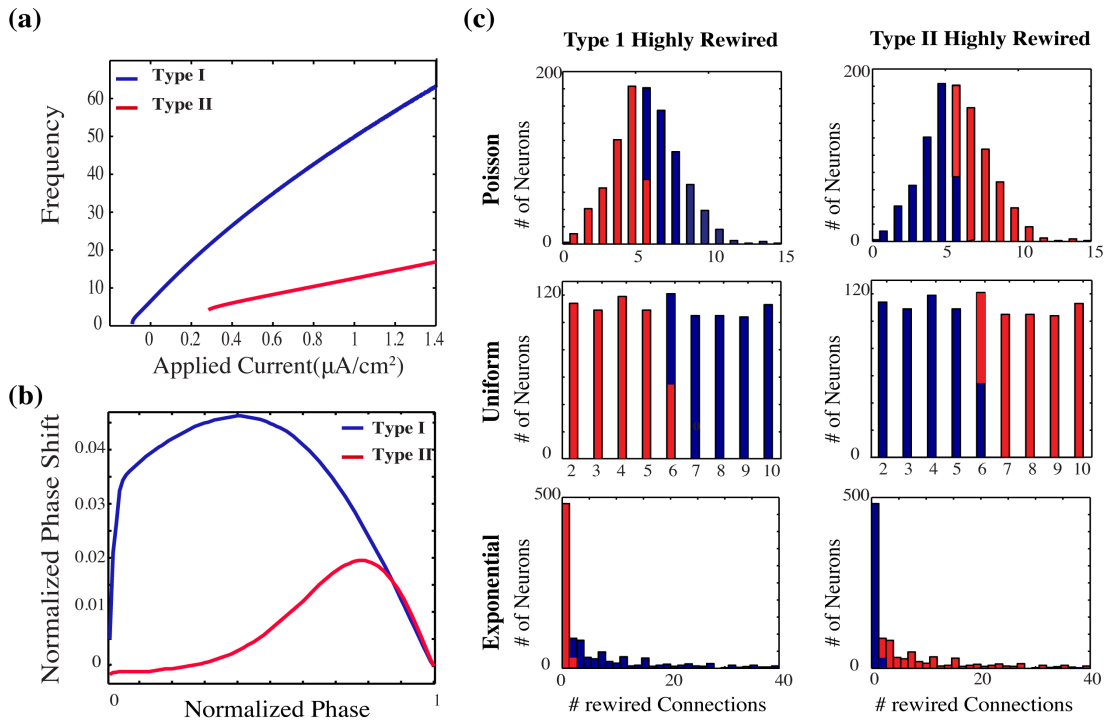

Figure 2.1 Excitability type and connectivity paradigm. a, b) Frequency-current (F-I) curve and phase response curve (PRC) for Type I (g_{Ks}=0.1, blue curve) and Type II (g_{Ks}=0.8, red curve) neurons. c) Histograms of the number of neurons with a specific number of rewired connections for the standard Poisson (top panels), uniform (middle panels) and exponential (bottom panels) connectivity paradigms for both Type I and Type II highly re-wired scenarios (for a mixed network of 50% Type I PRC and 50% Type II PRC). In Type I highly re-wired scenarios (left column of the panel c) neurons with the higher number of rewired outgoing connections have Type I excitability characteristics

(blue bars). Type II highly re-wired scenario is displayed in the right column of panel c, where Type II neurons have a higher number of rewired outgoing connections (red bars).

The presented results are obtained primarily for networks that all have on average p=0.15 global re-wiring fraction. Smaller global rewiring fractions resulted in very narrow distributions of re-wired connections, while higher rewiring probabilities led to global synchrony irrespective of the cell distributions (see Fig. 2.3).

Thus in the 'no variance' case, for a network of 1000 neurons with 4% connectivity density and average rewiring probability P=0.15, each neuron has exactly 6 re-wired connections. In the 'uniform distribution with a fixed variance' case, the average number of re-wired connections per neuron is 6, but it can vary across neurons by ±4, resulting in a uniform distribution from 2 to 10 re-wired connections per neuron (a range of ±4 was kept constant for other P values as well). In the 'exponential distribution' case, most neurons have none or few re-wired connections while a small fraction of neurons have the majority of their connections re-wired.

2.3.2 Synchrony and synaptic weight

To investigate the interplay between the statistics of network structure and cellular excitability in generating network dynamics, we compare two different regimes: (a) Type I PRC neurons Highly re-wired, in which neurons with higher rewiring probability are selectively assigned Type I excitability and those with lower rewiring probability have Type II excitability (Fig. 2.1c, left column), and (b) Type II PRC neurons highly re-wired, in which neurons with higher rewiring probability are selectively

assigned Type II excitability and those with fewer rewiring connections are Type I (Fig. 2.1c, right column).

Figure 2.2 shows results for these two cases in a network of 1000 excitatory cortical pyramidal neurons with 50% Type I and 50% Type II neurons. In figure 2.2a, the synchrony index (measured using the Golomb [99,100] synchrony measure for a 1s simulations, see the Methods section) is depicted as a function of synaptic weight when the average global rewiring fraction is P=0.15 and the intrinsic cellular frequency is distributed over the interval 15±2Hz. With each different connectivity architecture, the Type II highly re-wired (red curves) scenario exhibits significantly higher synchrony in comparison with the Type I highly re-wired (blue curves) scenario. In other words, if Type II neurons have more re-wired connections, they can lead both populations of neurons to synchronous activity, whereas if Type I neurons are those with more long-distance connections, they inhibit the emergence of synchronous spatio-temporal patterns. Note that in all of these simulations the number of out-going connections per neuron is fixed (40 connections) but neurons can have different numbers of re-wired connections. The biggest difference in synchrony for Type II highly re-wired versus Type I highly re-wired regimes occurs for the exponential distribution, which has the widest range of re-wired to local connections. In this regime, the excitability type of the few neurons that have all or most of their connections re-wired results in dramatically different network dynamics (Fig. 2.2b). It is notable that excessive increase in the synaptic strength can drive both Type I highly re-wired and Type II highly re-wired networks out of synchrony. This is primarily due to the mismatch of Type I and Type II firing rate, because of their disparate F-I curves.

In contrast to these mixed cell networks, the dynamics of homogenous networks composed solely of either Type I or Type II neurons (Fig. 2.3) are much less sensitive to variations in network connectivity architecture. Figure 2.3a displays the synchrony index for homogenous networks of Type I and Type II neurons as a function of synaptic weight for Poisson, uniform, exponential and no variance connectivity paradigms. The homogenous Type I networks show no signs of synchrony for any of the connectivity patterns (Fig. 2.3a,b). On the other hand, Type II networks show a significant tendency to synchronize, and increasing coupling strength leads to highly synchronous dynamics in all connectivity frameworks (Fig. 2.3a,b).

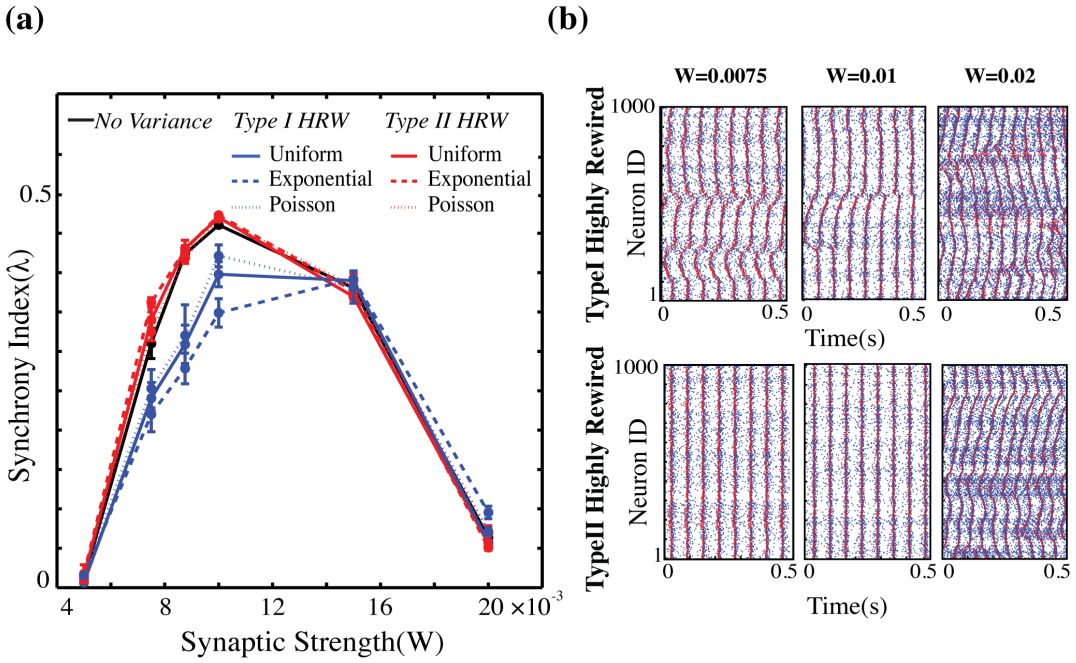

Figure 2.2 Synchrony in a heterogonous network of Type I and Type II excitatory neurons as a function of synaptic weight. a) Synchrony in a heterogonous network of Type I (50%), Type II PRC (50%) neurons as a function of synaptic strength for no variance (black solid line), uniform variance (solid lines), Poisson (dotted lines) and exponential (dashed lines) distributions for both Type I highly re-wired (Type I HRW shown in blue traces) and Type II highly re-wired scenarios (Type II HRW, red lines). These simulations have a rewiring probability of P=0.15 and frequency distribution of 15±2 Hz. b) Examples of raster plots (blue dot: Type I neurons, red dots: Type II neurons) for exponential distribution with synaptic strengths of W=0.0075, 0.01 and 0.02.

Here we see an extreme increase in the synaptic weight drives the network dynamics out of synchrony. The previously conducted studies have shown that increasing the firing rate of Type II neurons leads to the disappearance of the phase delay region of the PRC, adversely affecting network synchrony [97].

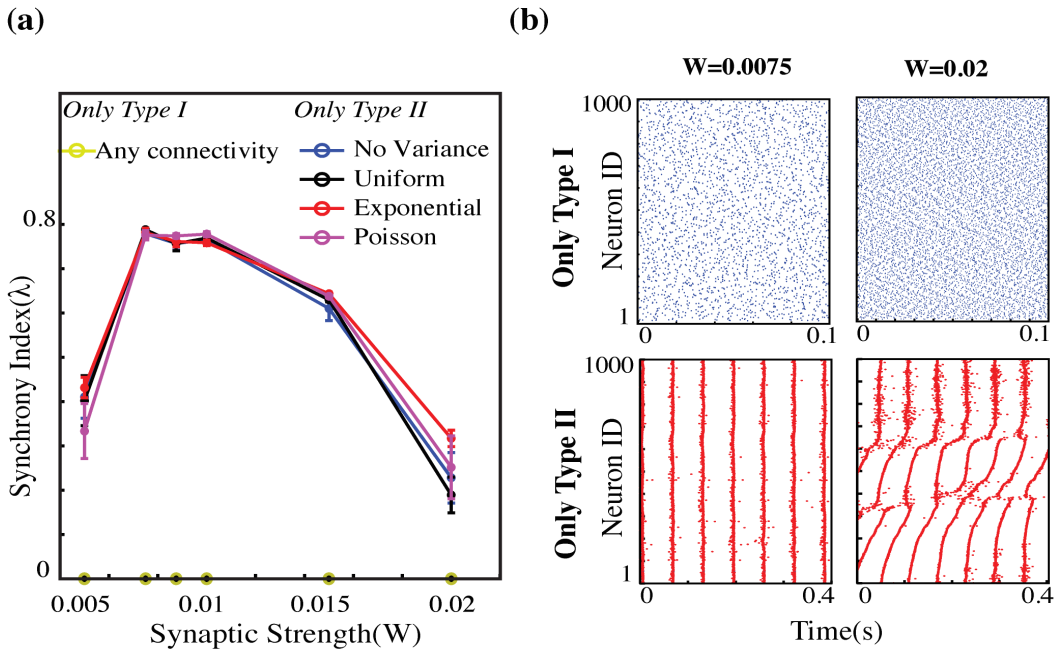

Figure 2.3 Synchrony in homogenous networks of Type I and II as a function of synaptic weight.(a) Type I PRC neurons display highly asynchronous dynamics, for all connectivity paradigms and for synaptic weight as high as w=0.02. Homogenous networks of Type II neurons, however, readily synchronize for small and intermediate synaptic strengths. (b) Examples of network activity for Type I (upper panel) and Type II neurons (lower panel). Note that time scales are different. Here the exponential connectivity paradigm was employed, with the same parameters for Type I and Type II simulations (P=0.15, frequency 15±2Hz, synaptic strengths of W=0.0075 (left side) and W=0.02 (right side)).

2.3.3 Synchrony and rewiring probability

These divergent effects on network synchrony are due to the interplay between individual neuronal properties and network architecture, and were robust for low values of average rewiring probability and for different fractions of cell types in the network. As illustrated in figure 2.4a, the

difference between Type I Highly re-wired and Type II highly re-wired scenarios (inset) is greatest for small values of average rewiring probability, namely P= 0.1-0.2, which is known to represent the small-world regime. As P increases further, synchrony increased overall, and the differences between scenarios decreased, due to the introduction of many random connections. Differences in network synchronization between rewiring scenarios were obtained when the fraction of Type II cells in the network was varied from 50% (Fig. 2.4b), with the greatest differences occurring when less than half of the cells were Type II (inset).

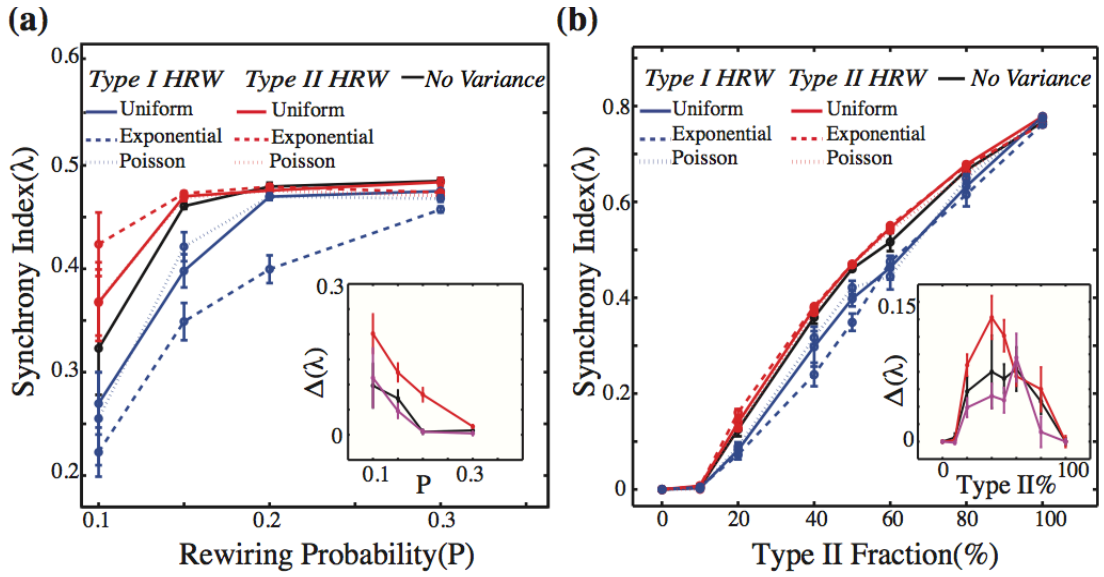

Figure 2.4 Synchrony as a function of rewiring probability and Type II fraction. a) Synchrony of a mixed network of 50% Type I PRC and 50% Type II PRC as a function of rewiring probability for no variance, uniform variance, Poisson and exponential distributions for both Type I highly re-wired (blue traces) and Type II highly re-wired (red lines) scenarios. In these simulations the average spiking frequency is 15±2Hz, with synaptic weight w=0.01. (b) Synchrony for a mixed network of Type I and Type II neurons, for different fractions of Type II neurons, where 0% Type II is a homogenous network of Type I and 100% is a homogenous network of Type II neurons (P=0.15, mean spiking frequency15±2Hz, and synaptic weights of 0.01). The inset shows the difference of synchrony index for Type II highly re-wired and Type I highly re-wired (black: uniform distribution; red: exponential, and pink for Poisson).

2.3.4 Synchrony and frequency Spread

We also examined the influence of heterogeneity in driving current on the difference in network synchrony between the Type II highly re-wired and Type I highly re-wired cases. While, the mean neuronal firing frequency remained 15 Hz, we varied its spread around that value. When heterogeneity is low, networks tend to synchronize regardless of their connectivity structure, but by increasing the heterogeneity, Type II highly re-wired networks show increased synchronization, with the greatest difference between cases occurring for a range of 12-18 Hz (spread of 40%) for intrinsic cellular frequencies. For larger heterogeneity in firing frequencies, networks with either rewiring distribution are not able to synchronize (Fig. 2.5a). The example raster plots for Type I highly re-wired and Type II highly re-wired cases for the exponential distribution and the Poisson distribution are displayed in figure 2.5b.

2.3.5 Synchrony in networks with high connectivity clusters

We also investigated the synchrony when clusters of either highly re-wired Type I cells or highly re-wired Type II cells were formed. We created a cluster from the predefined top fraction of highly re-wired neurons by interconnecting all neurons within that group. Here we set the initial network connectivity to be such that both types of networks, Type I highly re-wired and Type II highly re-wired (see Fig. 2.2a) do not show significant synchrony. We then added connections between preset fractions of the most highly re-wired group of neurons. In networks with Type I highly re-wired neurons, interconnecting up to 12% of the most highly re-wired cells did not appreciably change the degree of synchrony in the system (Fig. 2.6b left

middle panel). In the Type II highly re-wired networks, however, even a small fraction of additional connections induced increased network synchronization (Fig. 2.6b middle right panel).

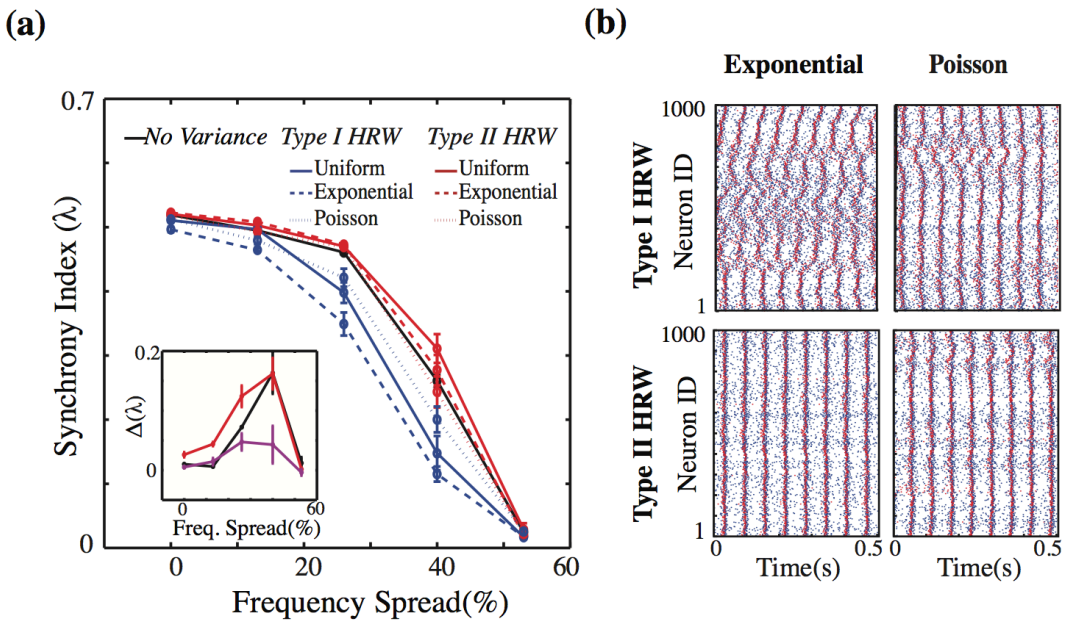

Figure 2.5 Heterogeneity in the driving current and the synchrony of mixed networks of Type I, and Type II. a) Synchrony of a mixed network of 50% Type I and 50% Type II neurons as a function of heterogeneity in the driving current for no variance, uniform variance, Poisson and exponential distributions for both Type I highly re-wired scenarios (shown in blue) and Type II highly re-wired scenarios (red lines) scenarios. These simulations have a rewiring probability of P=0.15 and synaptic weights of 0.01. The inset of Fig 2.5a shows the difference between the synchrony level of Type I highly re-wired scenarios (shown in blue traces) and Type II highly re-wired scenarios (red traces). The exponential and uniform distributions have a bigger gap than Poisson distribution between these two situations (black: uniform distribution; red: exponential, and pink for Poisson). b) Raster plots for Type I highly re-wired (upper panel) and Type II highly re-wired (lower panel) are shown for exponential (left side) and Poisson connectivity (right side) with spread of 40% in frequency.

Thus these results indicate that a clique consisting of a few Type II PRC neurons with long-distance connections can drive network dynamics toward synchrony, while a similar connectivity structure involving Type I neurons

does not facilitate the emergence of synchronous activity (Fig. 2.6a comparing red and blue lines).

To explore whether the emergence of synchrony was due to interconnecting Type II neurons, regardless of their connectivity, or whether the long-range connections made a difference, we performed simulations in which we interconnected Type II and Type I neurons at the bottom of the rewiring distributions (Fig. 2.6a green and purple traces). The uniform distribution, and particularly the exponential distribution, exhibited a significant difference in synchronization (red and green lines in the middle and bottom panels of Fig. 2.6a, respectively). The Poisson distribution (Fig. 2.6a, top panel) shows no significant difference. For the exponential distribution, forming a cluster of lowly re-wired Type II neurons resulted in the formation of domains of local synchronous activity, but overall level of synchrony was lower as compared to the case when the most highly re-wired Type II neurons formed a cluster (see raster plots marked IV and V in Fig. 2.6b).

In none of the distributions did interconnecting lowly re-wired Type I neurons result in higher synchrony (purple traces in Fig. 2.6a). These results show that the excitability type of the neurons within clique as well as statistics of their connectivity play an important role in facilitating the emergence of global synchrony.

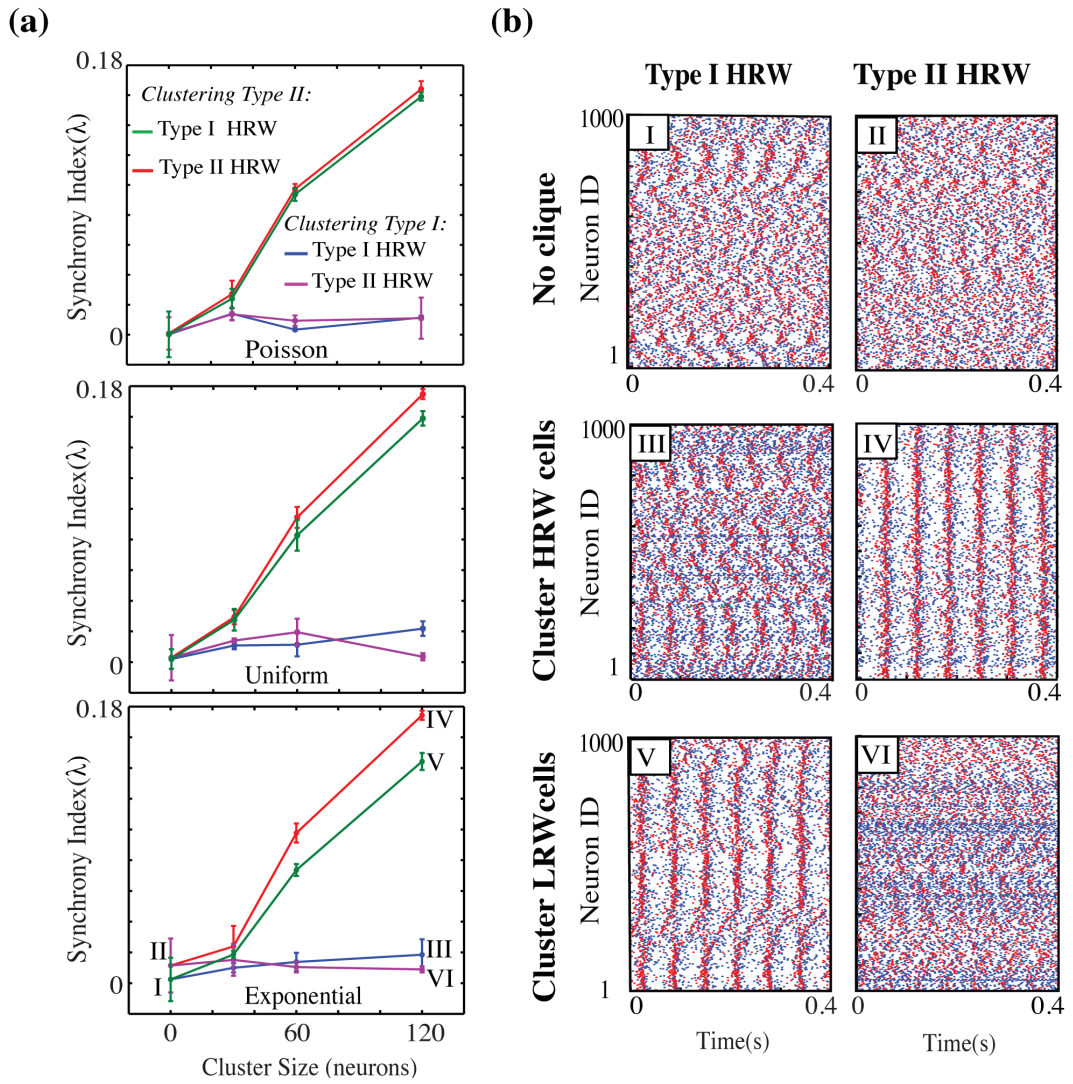

Figure 2.6 Implementing a higher order structure. a) Synchrony for mixed network of 50% Type I PRC and 50% Type II PRC with w=0.005, when we interconnect a fraction of most highly rewired (HRW, taken from the top of the rewired distributions) or lowly rewired (LRW, taken from the bottom of rewired distributions) neurons to form connected cliques in Poisson distribution (top panel), uniform (middle panel) and exponential (bottom panel) distributions for the both Type I highly re-wired and Type II highly Rewired cases. b) (top) Example raster plots for exponential distribution for both the Type I highly re-wired (left, marked I) and Type II highly re-wired (right, marked II) cases when no cliques are present. b) (Middle) Network activity when the top 12% of highly rewired neurons are additionally interconnected: left - Type I highly re-wired case (marked III), right Type II highly re-wired case (marked IV). b) (bottom row), Network activity when neurons with the *lowest* number of rewired connections are interconnected. In the Type I HRW scenario (left, marked V), the clique has Type II excitability and generates scattered patterns of synchronous activity. In the Type II highly re-wired scenario, the clique has Type I excitability (marked VI) and increases the network firing rate without affecting network synchrony.

2.4 Discussion

In this study we explored the interaction between excitability properties and local connectivity characteristics of individual neurons in affecting network synchronization. Namely, we investigated how the effects of structural network heterogeneities coupled with varying cellular dynamics can lead to modifications in network-wide activity patterns. The neurons in the network were allowed to have varying numbers of re-wired connections, while at the same time their excitability exhibited Type I or Type II characteristics. We varied the network distributions of re-wired connections per neuron between Poisson, uniform and exponential distributions. We show that highly re-wired cells of Type II excitability facilitate increased levels of network-wide synchrony. They form a distributed backbone in the network driving other cells toward synchrony. This effect was exacerbated in the re-wiring distribution having the longest tail (namely the exponential distribution). This distribution exhibited the greatest change in synchrony when the excitability type of the neurons with highest degree of rewiring was changed from Type I to Type II. This indicates that relatively few super re-wired Type II cells can significantly increase the level of network-wide synchrony, however increased synchronization is not realized when these highly re-wired cells have Type I excitability (see Fig. 4 a and b their insets).

The effects on synchrony being mediated by a small population of highly re-wired Type II cells is exacerbated when we allow these highly re-wired Type II cells to form connected clusters. In this case even a small Type II cluster, irrespective whether formed from highly re-wired cells or minimally

re-wired cells, drives a significant increase in network-wide synchrony. For exponential distribution networks, the difference in improved synchronization induced by clusters of highly re-wired compared to minimally re-wired Type II cells was greatest reflecting the large differential in the number of re-wired connections per cell at either end of the distribution.

Thus, our results indicate that heterogeneity in cellular connectivity, and subsequently not only first moment but also second moment of connectivity statistics, are important for spatio-temporal pattern formation in the network. This result may have significant implications for characterizing real-world network connectivity patterns, since often connectivity statistics are known only for a few identified cells. We show that relatively few cells of specific dynamical and connectivity properties can significantly change spatio-temporal patterning.

For example, these results may be pertinent when considering the modulation of neuronal excitability in the brain during sleep and wake states. It has been shown that intrinsic excitability of neurons can be modulated by acetylcholine levels [28]– high levels of acetylcholine (Ach), during waking and REM sleep, drives neuronal excitability towards Type I behavior, while the absence of Ach, during SWS sleep, pushes excitability towards Type II. We show that relatively few neurons expressing receptors that are sensitive to the Ach levels can dramatically change network-wide dynamics.

The synchronizing role of the Type II clusters maybe also is important to understanding pathological brain activity. It has been shown that upon an injury to the dentate gyrus, its circuits undergo architectural rearrangements,

which include formation of recurrent connections among excitatory granule cells. These changes make its circuit hyperexciatable and prone to generating epileptic seizures [101,102,103]. Morgan and Soltesz showed that even by keeping the number of connections constant throughout the network while assigning more connections to a few granule cells (GC) and interconnecting these hubs, they can create a circuit with hyper-excitable characteristics prone to generating seizure like activity [104].

CHAPTER III

Measuring Predictability of Autonomous Network Transitions into Bursting Dynamics

Understanding spontaneous transitions between dynamical modes in a network is of significant importance. These transitions may separate pathological and normal functions of the brain. In this chapter, we develop a set of measures that, based on spatio-temporal features of network activity, predict autonomous network transitions from asynchronous to synchronous dynamics under various conditions. These metrics quantify spike-timing distributions within a narrow time window as a function of the relative location of the active neurons. We applied these metrics to investigate the properties of these transitions in excitatory-only and excitatory-and-inhibitory networks and elucidate how network topology, noise level, and cellular heterogeneity affect both the reliability and the timeliness of the predictions. The developed measures can be calculated in real time and therefore potentially applied in clinical situations. *This chapter was published in PLOS ONE journal in* ***2015*** [88].

3.1 Introduction

The complex dynamics of brain networks underlies information processing as well as various pathologies. Epilepsy [105,106] and/or Parkinson's disease [93] are the most prominent examples of rapid autonomous transitions of network level spatio-temporal patterning from normal, largely asynchronous behavior into episodes of synchronous pathological activity that constitute underpinnings of the pathology. While, in the case of epilepsy, a significant fraction of seizures can be treated with medications or invasively with surgery, there is still large number of cases in which patients have to deal with a threat of impending seizures.

Therefore it becomes imperative to develop tools which, based upon online monitoring of brain dynamics can predict seizure, warn the patient, and/or optimally, take measures (through controlled drug infusion or electrical stimulation) to counteract dynamical changes in the network dynamics near the foci that lead to seizure onset.

There is a wealth of research being conducted that is centered on developing metrics and algorithms that would monitor changes in the brain activity (usually EEG signals or intracranial recordings) and predict impending seizures [107,108,109,110]. Existing measures have relatively low success rates providing a lot of false positives or false negatives [111,112,113,114]. Others analyzed the activity of network and individual neurons around the epileptic onset [80,115, 116,117,118].

In this chapter I take somewhat different approach. We developed a set of measures to study early spatial features of network reorganization upon

impending transition into bursting dynamics. Namely, we investigate whether and under what conditions we can identify and later detect early dynamical signs of transitions from synchronous to asynchronous dynamics in highly simplified settings. In loose terms we assume that the asynchronous mode of activity corresponds to interictal dynamics while synchronous activity corresponds to seizure itself. While this is clearly an oversimplification the goal of this chapter is to elucidate universal properties of transitions between those two modes of activity.

To make the settings at all relevant to possible clinical applications, the only information we utilize is the relative spatial positions of the neurons and their spiking activity patterns. This could in practice correspond to multiunit information obtained from two or more depth electrodes placed in the brain. We further assume that we have access to this information in the brain region corresponding to localized seizure foci and that transition in this region alone will generate distributed seizure dynamics.

We do not tackle the problem of how do synchronous dynamics spread throughout the brain. We investigate the aforementioned transitions within ring of excitatory only or excitatory- and-inhibitory integrate- and-fire neuronal networks. This model has been used for more than a century and still is widely used due to its low computational cost, broad range of applications, simplicity along with accuracy [7,119]. Even though that the LIF model is one of the simplest models of neuronal dynamics it can reproduce number of biologically observed spatiotemporal patterns depending on the connectivity, synaptic weights, inhibitory feedback, noise and heterogeneity. In 1991 Abeles, showed that if network wires randomly, tight temporal synchrony in order of milliseconds could be easily attained [120]. However,

Hopfield and Herz studied a network of locally connected integrate-and-fire oscillators neurons and they observed mostly asynchronous dynamics unless very late in the simulation (more than a hundred periods in a network) that invalidate any importance of synchrony in coding information comparing with biological short time scales of decision making [121]. This result was partially explained by D. Hansel et al, who investigated dynamics of purely excitatory homogeneous and fully connected networks of LIF and Hodgkin-Huxley model [122]. They showed that depending on the type of neuronal Phase Response Curve (PRC) excitation for neurons with Type I characteristic is mostly desynchronizing, however in neurons with Type II properties, excitation can lead to synchrony. Campbell and Wang (1999) on the other hand showed that network can reach synchrony much faster than the original estimate (within a few periods), they showed that the time needed to reach this synchrony is a logarithmic function of the network size [123]. At the same time it was recently shown that noise statistics itself could dramatically change neural spiking properties [124]. Brunel on the other hand investigated the effect of added inhibition into the excitatory oscillators [125]. He studied the dynamical properties of a network of sparsely randomly interconnected excitatory and inhibitory spiking leaky integrate-and-fire neurons. He showed that the networks could switch between synchronous and asynchronous activity, consisting of the propagating waves of activity, depending on driving frequency and excitatory-inhibition inter- actions. Along these lines, Tsodyks, et al. showed that excitatory-inhibitory network of LIF neurons that are interconnected with nonlinear synapses can adopt a synchronous activity associated with population bursts intermittent with long periods of asynchronous activity [126]. These types of transitions have been studied recently within the framework or extreme events [127].

3.2 Methods

3.2.1 Spiking Neuron Model

The Leaky integrate-and-fire (LIF) model was used to simulate network of excitatory and interacting excitatory-inhibitory neurons. The evolution of the voltage across the membrane of neuron 'j' is defined as follows:

$$\mathrm{C}\frac{\mathrm{d}V^j}{\mathrm{dt}} = -\alpha^j\left(V^j - E\right) + \mathrm{I_{ext}} + I^j_{syn} \tag{3.1}$$

Where V^j and C are the voltage and capacity across j^{th} neuron's membrane, respectively. The constant α is the leak conductance of the cell that is minimally different for each neuron and chosen from Gaussian distribution (μ=1, SD=0.05). Here I_{ext} is an externally applied current to each cell. Depending on the network model studied (i.e. whether the transitions are due to the noise or to the significant firing frequency mismatch) it can be identical for all of the neurons' external current that excitatory neuron receives: I^e_{exc} = 1.05 (the steady state is for most cells just above threshold), external current that inhibitory neuron receives: I^i_{exc}=0.95 (just below the threshold for most cells), or it can be taken from a uniform distribution (I^e_{exc}=1.05, SD=0.1 and I^i_{exc}=0.95, SD=0.05). After the electrical potential across the cell membrane achieves the threshold set to V_T = 1, the cell fires an action potential and its membrane potential is reset to V_{reset}. We set resting-potential 'E' and reset-potential 'V_{reset}' equal to zero. Immediately after neuron spikes, the cell enters the refractory period (T_{ref}=1.5ms). This synaptic input from presynaptic cell into the postsynaptic cell can be positive or negative depending on its excitatory or inhibitory character of the presynaptic cell and is defined as follows:

$$I_{syn}^{j} = \omega \sum A_{ij}(H(t) - H(t-\tau)) \quad (3.2)$$

Where i and j are presynaptic and postsynaptic neurons, respectively. The ω is the efficacy of connection between presynaptic and postsynaptic neurons; A is the adjacency matrix, H (t)-a Heaviside function, and τ=1ms represents the spike duration. We used Euler method with step size h≈0.01ms (estimated from time duration of the spike) to integrate LIF equation for the network. For networks dynamics incorporating stochastic component, we defined noise as a lighting bolt arriving randomly at each cell with predefined probability. Its arrival at a given site caused the cell to fire instantaneously independent of the membrane voltage, unless the cell was currently spiking or in its refractory time.

3.2.2 Networks Structures

The excitatory only network is composed of 200 excitatory neurons forming a 1-D ring structure. The small-world framework was used to vary continuously the network connectivity depending on the rewiring probability [45]. This rewiring breaks a local connection that comes from presynaptic neuron and forms a new random connection to any other postsynaptic neuron that didn't have connection before. Thus the network connectivity can vary from local connectivity (P_e=0), to the random connectivity (P_e=1). Every neuron establishes 8 connections to its neighbors (i.e. R=4).

For interacting excitatory and inhibitory systems we added a corresponding network of 200 inhibitory cells. Thus here the network connectivity pattern is defined by two parameters (P_e and P_i). Every excitatory cell makes 8

connections to other excitatory and inhibitory cells, every inhibitory cells makes also 8 connections to both other inhibitory and excitatory neurons. The synaptic weight for connections originating from excitatory cells is ω_e=2.2, while that of inhibitory neurons ω_i=0.8.

3.2.3 Analysis

In order to identify type of the networks' dynamics (asynchronous versus synchronous) and characterize their transitions, we created a measure based on the relative timing of each neuron's with respect to other neurons in the system (T_D). We divided time of simulation into number of equal length time-windows. The length of the time-window was set to be the average spike frequency in the network. At each time window, the minimum time difference between every neuron's spike within that window and all other cells is computed (regardless whether the other cells spike within that time-window). If there is more than one spike per neuron in a time window we choose the earliest spike's time for the given neuron. This calculation is repeated for all the consecutive time windows. These times are then sorted based on the physical distance between neurons and the histogram of the mean times at every distance is resulting in distinct spatial vector T_D generated for every time window. The example of T_D is illustrated using a color plot on figure 3.4, where vertical axis represents the distance between two neurons; horizontal axis is showing the time of simulation. The color scale indicates the T_D values. We define T_M as (spatial) average of T_D and use its value to detect temporal location of the transitions into and out of the

bursting regime. To characterize the properties of the T_D vector near the transition point we calculate its spatial derivative d T_D. Finally we calculate dT_M, which is the average value of dT_D and also variance of T_D and d T_D.

3.2.4 Onset and slope of the transition

We want to use measures characterizing properties of T_D to detect precursors of the transitions into the bursting dynamics. We calculate the values of the abovementioned measures in the time windows immediately preceding the onset of the bursts (as defined by the T_M). We then calculate the ratios of the measures progressing forward in time. Therefore we calculate $R_N=M_{N+1}/M_N$), the ratio of the (generalized) measure 'M' calculated 'N' time-windows before the burst onset (N = 0, 1, 2, 3, 4, 5). If the R_N is significantly different from unity we assume that spatial patterning within this time window is persistently and significantly different from that in the prior window. The lead-time is defined as the number of time windows prior bursting onset within which the spatio-temporal network pattern undergoes significant change with respect to the one observed in a window before. This lead-time is then averaged over many realizations of bursting transitions.

3.3 Results

3.3.1 Characterization of network dynamics

We first characterize the simplified neuronal network dynamics and investigate how distinctive network properties such as the connectivity structure, noise and inhibition can shape its dynamics and influence the properties of transitions between different modes of activity patterns. Here we generally differentiate transitions from/into bursting regime to be driven by noise (modeling uncorrelated input from other parts of the network) and, separately those generated internally by the network, caused by distribution of cell intrinsic frequency.

3.3.2 Excitatory networks with deterministic and noise driven dynamics.

First we investigated the dynamics of a network consisting of 200 integrate-and-fire excitatory neurons in 1D ring structure and examine its spatio-temporal patterning as a function of noise, external current and its underlying connectivity pattern. The neurons are set to fire spontaneously as they are driven by constant current or random input. The three stimulation types are intended to simulate cellular changes due to the intrinsic neuronal excitation (constant current), input coming from other brain modalities (random input), or both.

It is well established that the dynamics of a neuronal network is highly dependent upon its structure; here we use small-world paradigm to vary network connectivity using excitatory rewiring probability $P_{e.}$ Accordingly,

here we show three major classes of network activity pat- terns can be formed for local, small-world and random topology in figure 3.1a–d respectively. The panels depict raster plots (left column; blue dots denote action potentials) and histograms (right column) of interspike Intervals (ISIs) associated with fully deterministic dynamics (no noise) of networks having different connectivity patterns. For P_e=0 (Fig 3.1a), i.e. for networks having exclusively local connectivity, we observe low frequency propagating chains of activity. Given that there is no input noise in the network, and the fact that a constant external current initiates the activity, one can observe repetition of the traveling wave-forms over time. The corresponding ISI histogram is very narrow.

Figure 3.1b depicts activity around the small-world regime (P_e=0.15), where most connections are local and few of them are rewired to form long distance connectivity. The Small-world regime is known for high clustering and short path lengths and has been shown that the brain possibly shares these connectivity features [46,48,128,129,130].

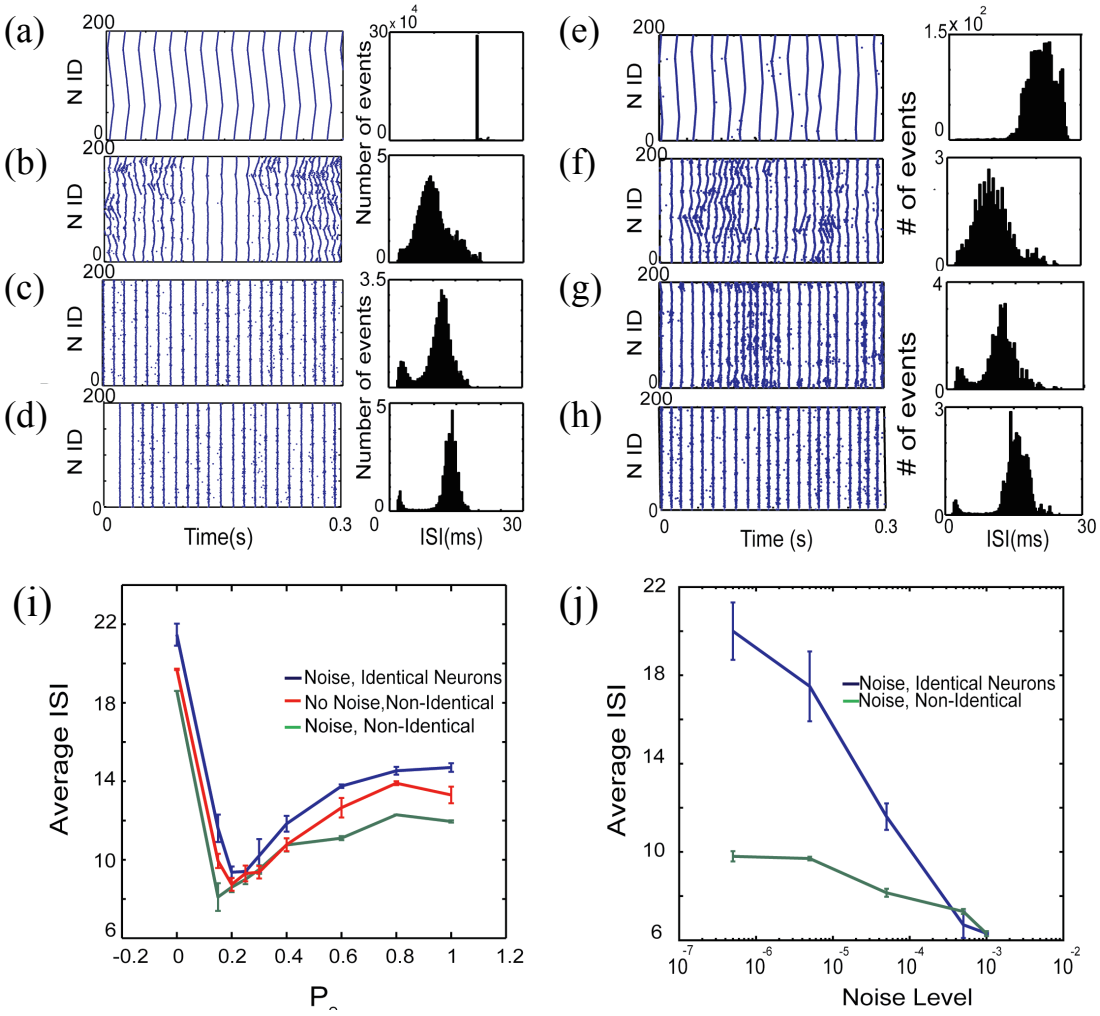

Figure 3.1 Dynamics of a network of 200 excitatory integrate-and-fire neurons with deterministic (left column) and noise-driven (right column) dynamics. (a-d) Raster plots and ISI histograms associated with deterministic dynamics of networks having P_e=0, 0.15, 0.4 and 1 respectively (blue dots denote timing of neuronal action potential). (e-h) Same as panels (a-d) for noise driven networks (noise frequency = 0.00005). (i) Changes of mean ISIs as a function of rewiring parameter for noise driven identical (I^e_{ext}=1.05, f_N=0.00005 blue line), non-identical (I^e_{ext}=0.95–1.15, f_N=0.00005, green line) and deterministic dynamics for non-identical neurons (I^e_{ext} = 0.95–1.15, red line). (j) Changes in mean ISI duration as a function of noise level for an excitatory network with P_e=0.15 for both identical (I^e_{ext}=1.05, blue line), and non-identical neurons (I^e_{ext} = 0.95–1.15, green line)[84].

The associated dynamics consists of two phases (Fig. 3.1b): 1) short irregular propagating waves of activity that collide occasionally and, 2) globally synchronous activity. At the same time, addition of few random connections causes ISIs to shift toward lower values reflecting the higher firing frequency. These kinds of dynamics were reported earlier and were also observed in various brain modalities during normal function and pathology [131,132,133,134,135]. With P_e=0.4, random connections are frequent enough to transform the dynamics into a single synchronized phase. Interestingly in the ISI histogram we see two distant peaks the main peak corresponds to the dominating low-frequency synchronous activity patterns, whereas the small high-frequency peak is due to the asynchronous activity appearing sporadically.

Finally, figure 3.1d illustrates networks with exclusively random connections (P_e=1). Where, we observe stable synchronous bursting with frequency much lower than the small-world regime. Figure 3.1e–h correspond to the same network structures as those presented in figure 3.1a–d, respectively, but with the addition of the background noise (please refer to methods). Here, the spatio-temporal patterning is similar to the fully deterministic case, with generally shorter episodes of bursting dynamics, more rapid transitions into and out of those regimes and more pronounced episodes of asynchronous dynamics especially for those P_e values around the small-world region.

Changes in the mean ISI values as a function of rewiring parameter are plotted for deterministic dynamics of non-identical neurons and noise-driven dynamics of both identical and non-identical cells (Fig. 3.1I). The general

pattern for all cases is similar, large ISI for local connectivity pattern (P_e=0.0), followed with a significant drop for small-world connectivity regime (P_e=0.15–0.2), and then increase of ISI values in more random network topologies (P_e>0.3). This data shows that firing rate is somewhat higher when both heterogeneity and noise present (green line) at P_e=0.15, and it reduced and shifted to P_e=0.2 either with eliminating the noise (red line) or heterogeneity (blue line). Albeit not surprising that the overall frequency increases with addition of noise (additional excitatory input), it is interesting that the frequency changes are more pronounced for random and local network connectivity than the small-world regime. The noise effect on ISIs values for both identical (I^e_{ext}=1.05, blue line) and non-identical neurons (I^e_{ext}=0.95–1.15, green line) are shown in (Fig. 3.1J). For the intermediate and low values of noise, the cell heterogeneity significantly lowers the average of ISI while for the higher levels of the applied noise there is no significant difference in the firing rates.

Here we will be primarily interested in characterizing transitions between bursting and synchronous activity patterns for different network cellular and network properties. To better illustrate the transitions between the synchronous and asynchronous regime we plotted raster plot with and example of such transition (Fig. 3.2a) together with cumulative signal of network activity (Fig. 3.2b) and example of voltage traces (Fig. 3.1c) near the transition point.

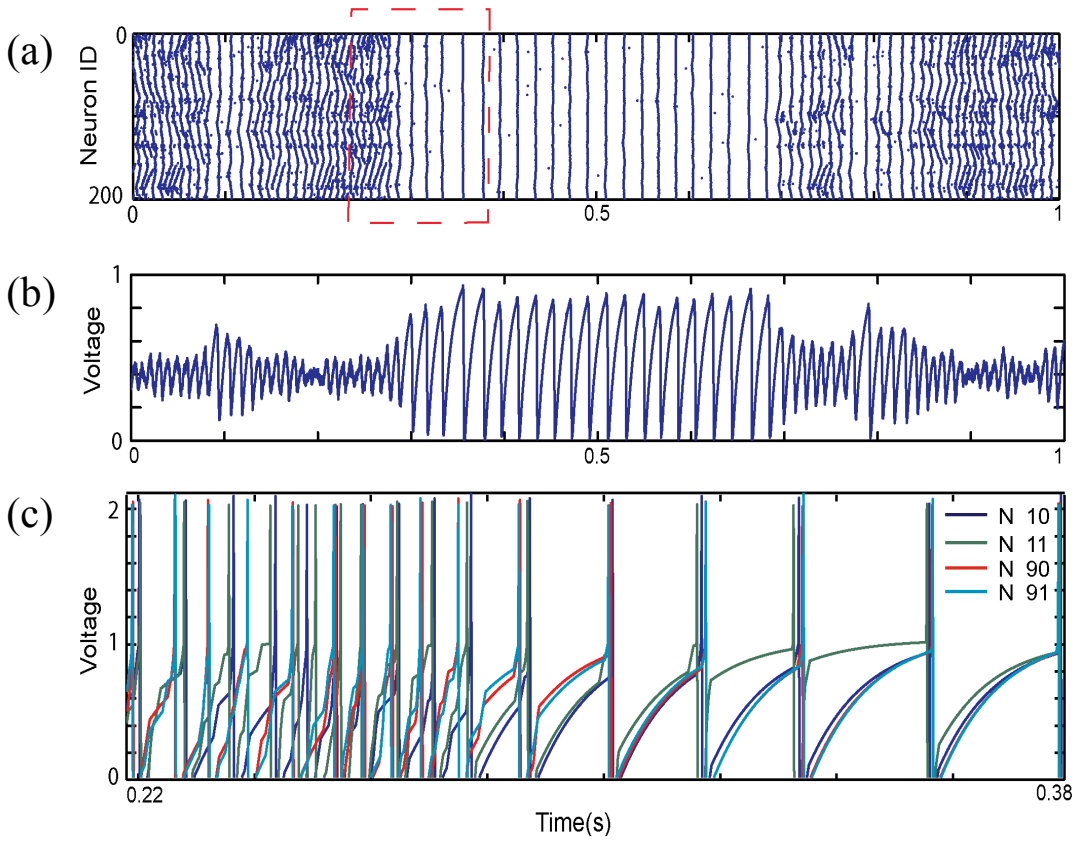

Figure 3.2 Network activity and individual neurons' voltage profiles before and after transition into synchronous dynamics. (A, B) An example of raster plot and cumulative network activity pattern for a system composed of 200 excitatory neurons, transitioning from asynchronous to synchronous dynamics. (C) Example of voltage traces of two pairs of neurons ([10, 11], [90,91]) where neurons in each pair are neighbors but the pairs are distant from each other[84].

Depicted example corresponds to the network where neurons obtain constant input. We observe, not surprisingly, that the pairs on neurons lying in spatial proximity are generally more synchronous that those positioned far from each other. Furthermore one can observe that during the asynchronous period the dynamics of the pairs is driven by mostly common asynchronous signal causing their activity to desynchronize, while during bursting they respond collectively to large network input.

3.3.3 Excitatory-Inhibitory networks with deterministic and noise driven dynamics.

Next, we investigated how the various topologies of inhibitory connectivity affect the network's spatio-temporal patterning. In order to do so, we created two corresponding rings of excitatory and inhibitory cells. The inhibitory neurons send same number of connections as excitatory neurons to other inhibitory and excitatory neurons, but their synapses are weaker than those originating from excitatory neurons. Inhibitory neurons are connected using the same framework as excitatory cells—initially these neurons are connected locally and then rewire part of those local connections based on the inhibitory rewiring parameter (P_i), figure 3.3a**.** To look at the effect of inhibitory network's connectivity pattern on the excitatory dynamics, we kept the excitatory rewiring parameter (P_e) fixed and varied the inhibitory rewiring parameter (P_i=0–1). Figure 3.3 presents results for the case when P_e=0.15. In case of local inhibition (Fig. 3.3c) we observed a strong suppression of propagating chains of activity in excitatory network in comparison with the excitatory only network dynamics (Fig. 3.3b). This suppression is evident during asynchronous activity regimes. The shape of synchronous burst does not change significantly.The increase of the inhibitory rewiring parameter (P_i) causes complex changes to the spatio-temporal firing pattern of the excitatory cells (Fig. 3.3c–e). The firing chains within the asynchronous dynamics increase in length, however at the same

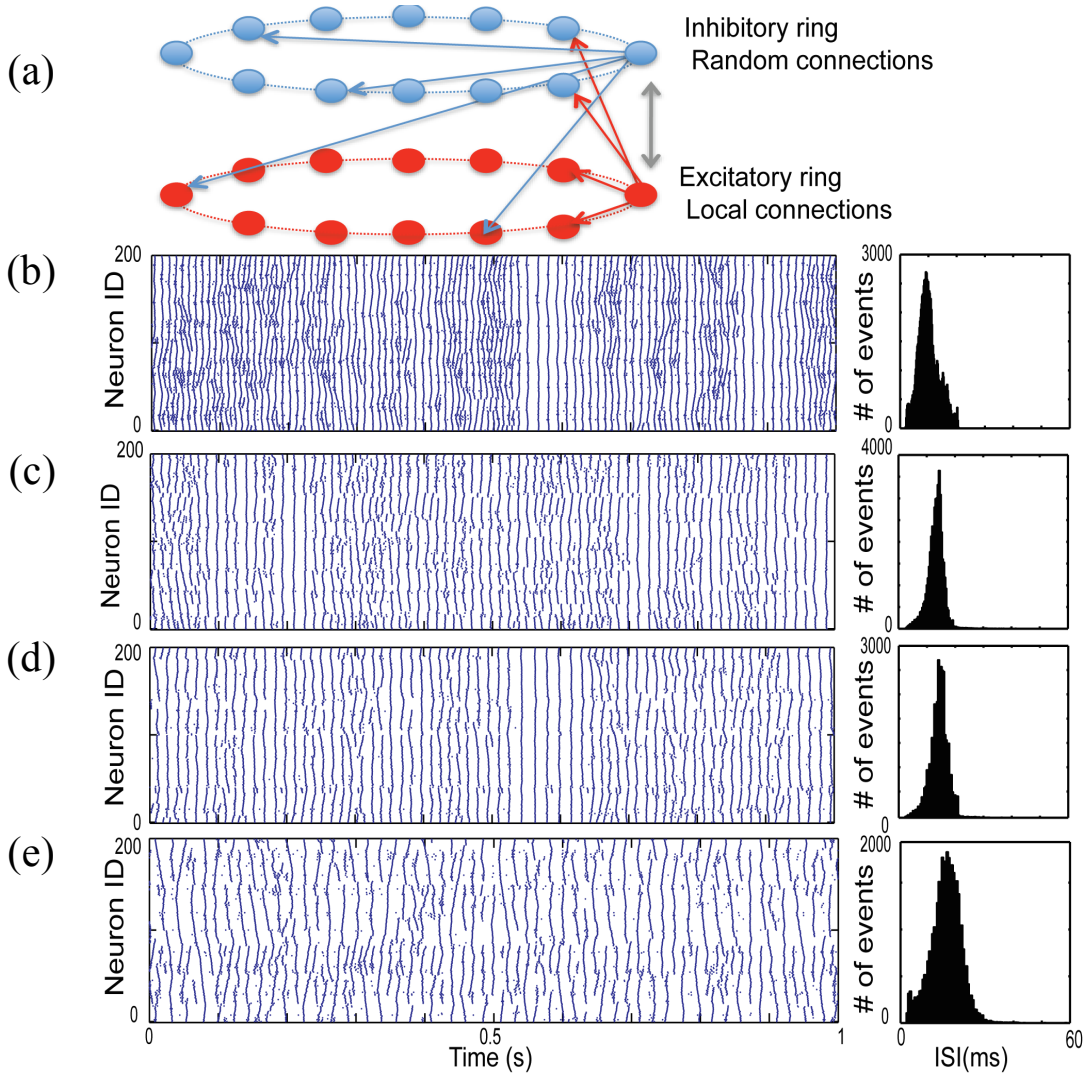

Figure 3.3 Interaction of excitatory and inhibitory networks for varying inhibitory connectivity in networks with deterministic dynamics. (a) Topology of interacting network of excitatory and inhibitory neurons. Here $P_e = 0.15$ and inhibitory connectivity changes from local ($P_i=0$) to random ($P_i = 1$). (b) Excitatory only neurons with $P_e = 0.15$ when there is no inhibitory feedback. (c) $P_i = 0$, (d) $P_i = 0.2$, the local propagating waves in the asynchronous regime are destroyed. (e) Random inhibitory connections ($P_i=1$), the firing frequency reduces significantly, while the propagating waves are longer and the synchronous bursting is suppressed.

time the synchronous bursts become suppressed for high P_i values (see Fig. 3.3e). Furthermore, the overall frequency of the firing tends to decrease with

P_i. This is due to rapid spread and equalization of inhibition through out the network.

3.3.4 Identification and quantification of observed dynamical regimes

As we showed above, networks having different properties such as underlying structure, noise and different inhibitory connectivity pattern exhibit distinctive dynamics. In most regimes however we do observe periodic transitions from asynchronous (or less synchronized) to synchronous (or more synchronized) modes of activity. We set out to characterize these different patterns of activity and ultimately elucidate the predictive dynamical features of transitions between these dynamical regimes. In particular we want to investigate under what conditions (if any) these features can be identified sooner rather than later, and thus, reversing the question, can they tell us something about the underlying network properties.

Since the changes in network activity patterns are rapid, we cannot apply measures that are based on long temporal averages, as this would obscure the transition detection. Thus, to characterize the dynamics we developed a set of measures based on assessment of instantaneous changes in adjacent spike-timings of neurons. Based on the observations reported in previous section, the underlying idea of the proposed measures is to analyze, instead of changes in temporal distributions, instantaneous properties of spatial distributions of neuronal activity in given time windows. The major advantage of the developed metrics is that they are simple to compute based

on the data that is readily available from recordings and thus can be applied directly to in vivo or clinical measurements. While the exact positions of the recorded cells are clearly unknown, one can ultimately divide the neural populations as coming from the same electrode (cells are nearby) and coming from other electrodes placed at various distances.

The specific question we want to answer is if, and if so, how much before the ultimate synchronous state can we detect changes in spatial network activity patterns. Also, we want to elucidate nature of this transition (e.g. is it a nucleation of locally synchronized groups of neurons)?

Here we divided the spiking data is divided into equal size time-windows with their duration matching the mean ISI observed in the network. Next, we calculate the time difference between closest (temporarily) spikes of every cell that fired within given window and every other cell in the network. These spike timings are then sorted based on the actual spatial distance of neurons (Fig. 3.4a)—below we will refer to this vector as T_D. We then aim to statistically characterize the properties of this vector as a function of network state, and more importantly near the impending transition into bursting.

Figure 3.4 shows an example of the raster plot (Fig. 3.4b) and computed T_D vector for the consecutive time windows (Fig. 3.4c). The color scale denotes the time difference between the spikes (note that scales are significantly different for different network structures). Figure 3.4d depicts the spatial derivative of T_D (dT_D), while figure 3.4e is the mean of T_D for a given time window (T_M). We will use the T_M to identify the onset and offset of the bursting regime. We do this by setting a threshold value of T_M below which

we considered that the network dynamics is largely synchronous. While this is to some extend arbitrary the results presented below are (within a range) largely independent of the exact value of the threshold chosen. The dotted line on figure 3.4e denotes the threshold of transition between the two (asynchronous and bursting) regimes. One can easily observe, that the values of T_D are highly dependent on the distance between the cells. The universal property for all network structures (except when P_e=1, see below) is the rapid loss of this distance dependence during the transition. We aim to statistically analyze and characterize properties of these transitions.

The developed metric is quite sensitive to the changes in the network dynamics across various network structures and detects even small variations in the overall observed pattern of activity. An example of such is presented in figure 3.6. This figure depicts changes in relative neurons' firing pattern as a function of their relative distance reported by the T_D, for various connectivity structures of excitatory network (P_e=0; 0.15; 1.0). While the network spatio-temporal patterns are significantly different in the three cases, the metric picks up the bursting regime without difficulty. Moreover the internal structure of the T_D vector can shed the light on the intra-burst dynamics of the network.

The spatial extend of the changes in T_D provides information about the correlation lengths between neuronal activities generated by propagating waves in the network. Thus when all connections are local and the average timing difference between spikes of neurons grows with their actual distance consistent with the long traveling chains of neuronal activities (Fig. 3.6a). On the other hand, when the network has small-world connectivity pattern

(P_e=0.15), we observe much more complex correlation structure with significantly decreased correlation length.

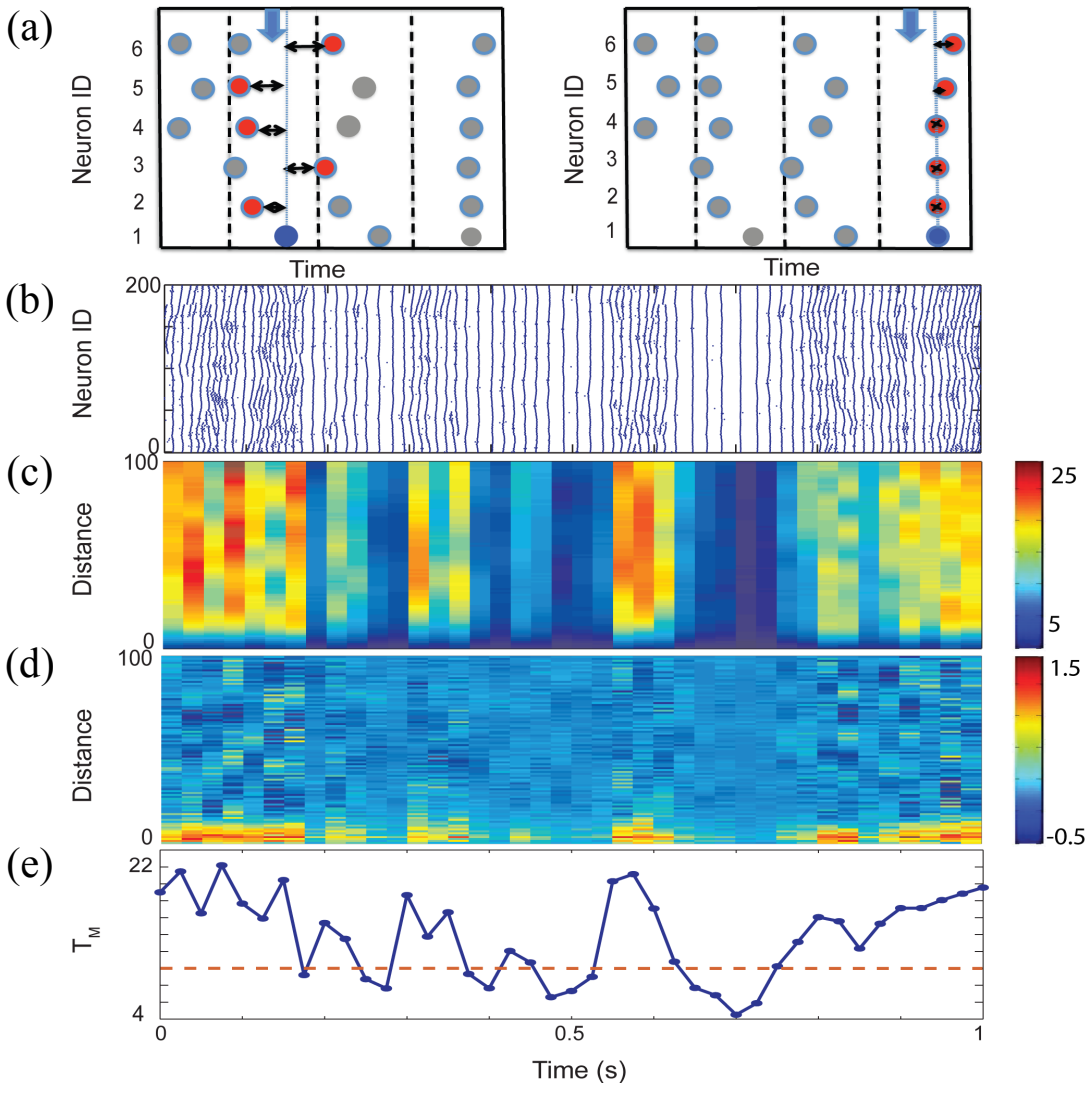

Figure 3.4 Characterization of the spatio-temporal dynamics of the network. (a) To characterize instantaneous spatial patterning in the network, we calculate the minimum time interval between each neuron's spike in the time-window (blue filled circles) with all other neurons' spikes and sort these timings based on their spatial distance. The left side of panel A shows the calculation for the a time window that has a asynchronous

activity with relatively large and highly variable time intervals; the right side panel depicts calculation for the time window with a synchronous activity and minimal time differences between the spikes. (b) An example of raster plot obtained from noise driven excitatory only network P_E=0.15,noise frequency f=0.00005(c) Color plot of consecutive T_D calculations; colors indicate the closest timing between spikes of neurons in the given window with all other neurons in the network. (d) Spatial derivative of T_D (dT_D) in each time window. (e) Mean of T_D for consecutive time windows (to which we refer as T_M). The dotted line is a cutoff, which we will use to identify the initiation of the bursting dynamics.

The distribution of the local extrema in the T_D again corresponds to the shorter chain lengths of activity in the raster plot (Fig. 3.6b). Finally, when all the connections are random (P_e=1), one can still observe changes in timing differences allowing for differentiation of dynamics between less and more synchronous network states. However there is no internal correlation within the given T_D. In figure 3.6c we pick few time-windows and show how these relative timings change as a function of actual distance for different structures: local, small- world and random. In case of local connections these timings increase monotonically with in- creasing spatial distance while in small-world structure there are local maxima and minima corresponding to the size of broken traveling chains. Finally in case of solely random connections there is no clear relationship between spike timings and spatial distance. In figure 3.6d we showed changes in spatial derivatives for the same time windows.

3.3.5 Characterization of dynamical regimes using the developed metrics.

First we set out to investigate the duration of the two (asynchronous and bursting) network regimes. We use the evolution of T_M to detect network

durations in respective regimes. The threshold defining the onset of the bursting regime is set arbitrarily, however its specific value did not influence significantly the obtained results. We studied duration of the bursting regime for both excitatory only and excitatory-inhibitory networks as a function

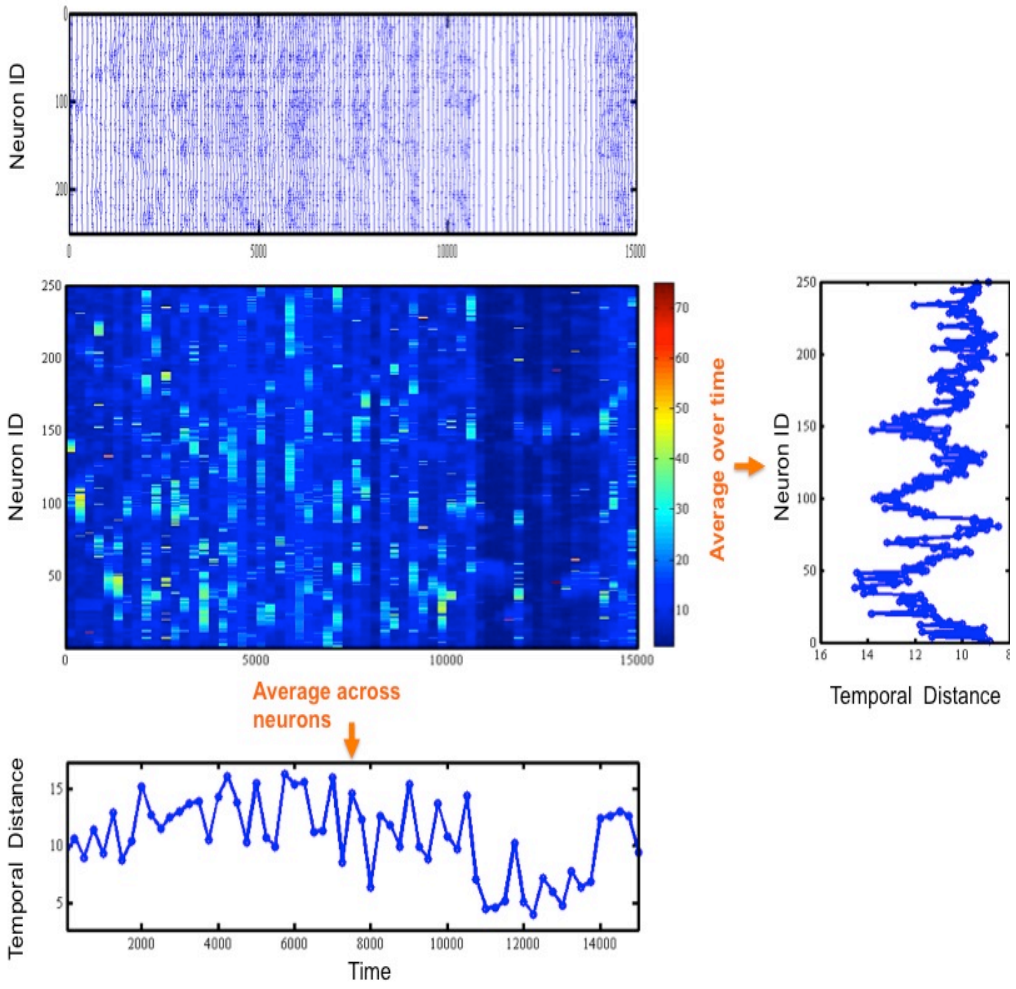

Figure 3.5 Sorting temporal distances based on neuron ID. Here all the temporal distances are sorted based on the neuron ID, where deep blue represents synchronous activity and brighter colors for less synchronous activity (middle left). The average this temporal distances across neurons at each time-window it creates a measure distinguishing synchronous versus asynchronous dynamics (bottom trace). However, the average of these temporal distances over time for each neuron distinguishes neurons that are initiating asynchronous dynamics (right trace).

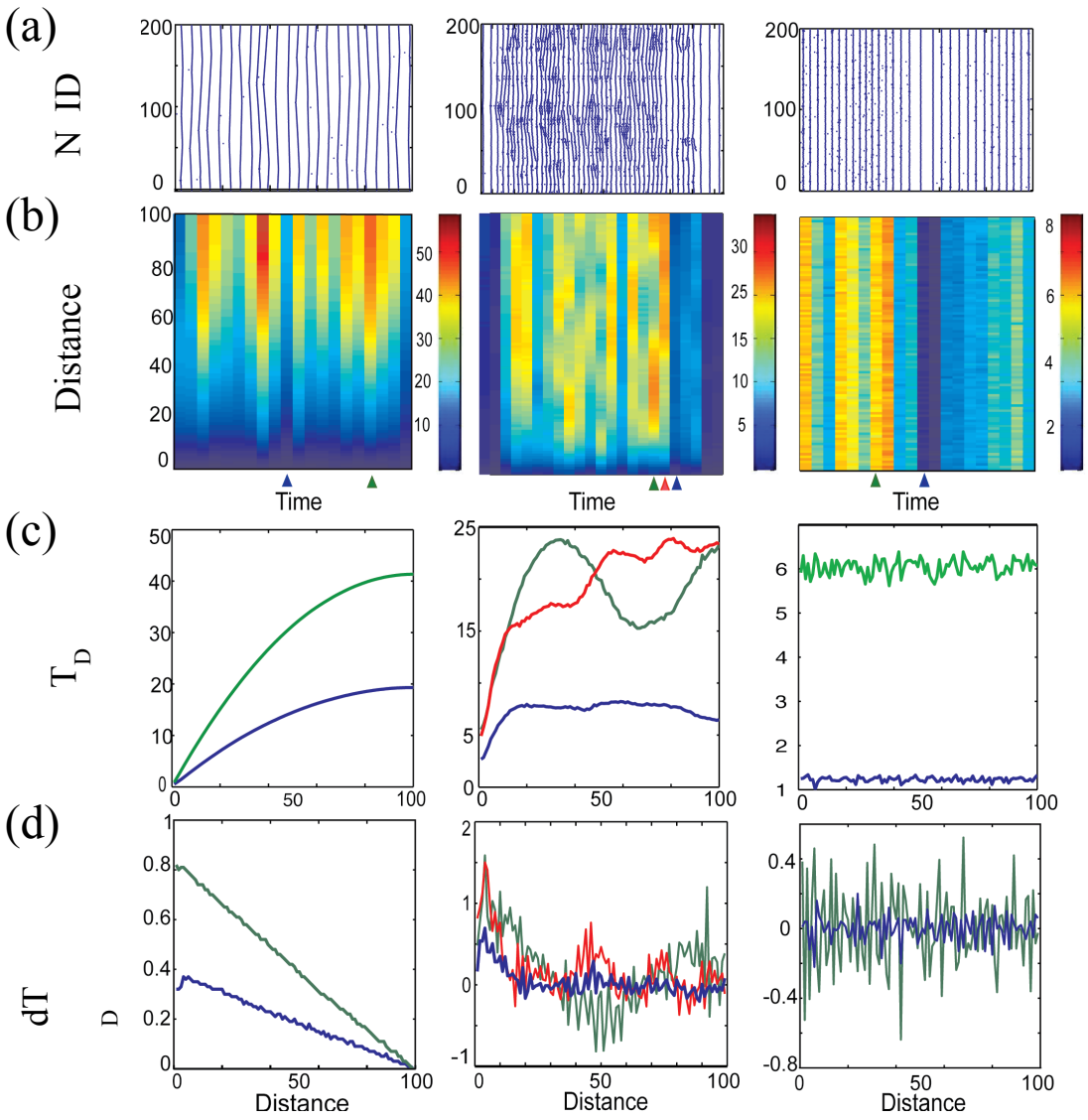

Figure 3.6 Raster plots and corresponding T_D and dT_D for selected time windows in an excitatory network. Where the left, middle and right column are associated with $P_e = 0$, $P_e = 0.15$, $P_e = 1$ respectively. (a) Raster plots; (b) Spatio-temporal changes of T_D; (c) Examples of T_D evolution with distance for selected time windows (marked of b); (d) examples of derivative of T_D at the same time points.

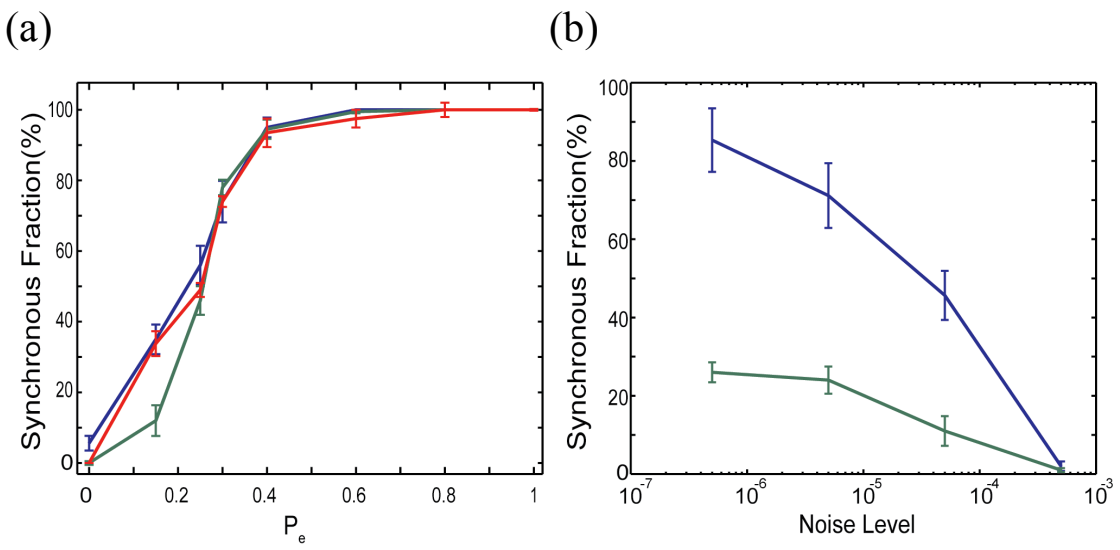

Figure 3.7 Characterizing the effect of noise level and connectivity structure on the dynamics of excitatory network. Characterizing the effect of noise level and connectivity structure on the dynamics of excitatory network. (A) Fraction of time network adopts synchronous dynamics as a function of rewiring parameter for noise driven identical (I^e_{ext} =1.05 for all neurons f_N=0.00005, blue line), non-identical (I^e_{ext} = 0.95–1.15, f_N = 0.00005, green line) and deterministic dynamics for network of non-identical cells (I^e_{ext} =0.95–1.15, red line). (B) The effect of the increasing noise level on the dynamics for the excitatory-only network with P_e = 0.15 for noise driven identical (I^e_{ext} = 1.05 for all neurons, blue line) and non-identical (I^e_{ext} = 0.95–1.15, green line).

of topologies of both networks and also as a function of noise level. Figure 3.7 shows the fraction of time spent in the bursting regime for excitatory only networks as a function of these parameters. Figure 3.7a reports this fraction as a function of network connectivity (P_e) for three types of networks. The first are the networks composed of identical neurons (same driving excitatory current I_e=1.05; see methods) having transitions between synchronous and asynchronous dynamics driven by the noise (f_N=0.00005). The second network type is not driven by noise, but at the same time its elements are not identical in terms of their driving current and thus their

intrinsic firing frequency (I_e=0.95–1.15; note that the mean I_e = 1.05). Eventually the third one is driven by noise and its neurons are non-identical in terms of the driving current (f_N=0.00005, I_e=0.95–1.15; mean I_e=1.05, green line). As observed earlier (Fig. 3.1) the fraction of time spent in synchronous regime increases significantly with increasing P_e. At the same time, for small-world regime, heterogeneity of neurons along with noise (Fig. 3.7a, green line) considerably lowers the fraction of time spent in synchronous dynamics. However, there is no significant difference between noise driven transitions and those cause internally by cell heterogeneity. For higher P_e values (P_e>0.3), the neuronal heterogeneity nor/and noise does not change the duration of bursting dynamics significantly.

On the other hand the effect of noise on the dynamics for the excitatory network is illustrated in figure 3.7b. Here we vary the noise level (i.e. the probability of occurrence of random spikes) for the two networks: those having identical driving current applied to all cells (blue line) and those having driving current randomly chosen from a distribution I_e = 0.95–1.15 (green line). The fraction of time spent in synchronous dynamics is suppressed with the increased levels of noise, but also depends strongly on cellular heterogeneity.

We analyzed in similar fashion the effect of the inhibitory topology on the spatio-temporal dynamics of the excitatory network (Fig. 3.8). As before we investigated the dynamics of three types of networks—the noise driven dynamics of networks composed of either identical neurons, non-identical neurons and fully deterministic dynamics of networks composed of non-identical cells (both excitatory and inhibitory). The mean driving current of

the inhibitory cells was set to be I_i =0.95—effectively below spontaneous firing threshold. Thus their firing was driven only by the excitatory network and/or noise. The connectivity of the excitatory networks was kept constant at P_e=0.15 and we varied the inhibitory connectivity (P_i=0.0–1.0). Interestingly the small-world regime of inhibitory connectivity corresponds to the largest fraction of time spent in synchronous dynamics (Fig. 3.8). As expected overall fraction of time that network spent in synchronous dynamics is lower in the presence of both noise and heterogeneity (green line). It is interesting to note that network spends most time in synchronous bursting regime when P_i=0.15 (small world topology) and it significantly decreases for random inhibitory network structure. This could indicate that changes in overall inhibitory network structure for example due to axonal sprouting could lead to network more prone to bursting.

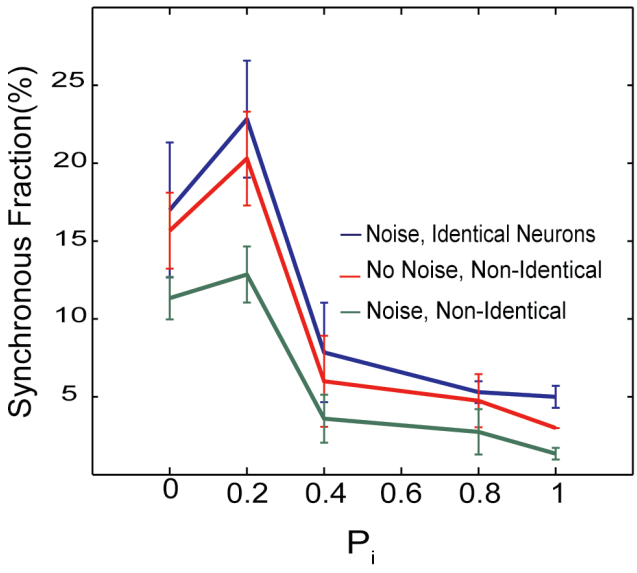

Figure 3.8 Fraction of time that the network spent in the synchronous regime. The synchronous fraction of dynamics as a function of inhibitory connectivity when excitatory connectivity is in small-world regime (P_e = 0.15), for: 1) noise driven identical neurons (f_N = 0.00005, I_e = 1.05,I_i = 0.95; blue line), 2) non-identical neurons (f_N =

0.00005, I_e = 0.95–1.15, I_i = 0.9–1.0; green line), and 3) deterministic dynamics of non-identical neurons (no noise, I_e = 0.95–1.15, I_i = 0.9–1.0; red line).

3.3.6 Network transitions from asynchronous to bursting regime.

The ultimate goal of this chapter is to characterize network transitions and their predictability from asynchronous activity into the bursting regime. Here we limit the meaning of predictability to identification of first signs of transition to bursting dynamics before the transition itself takes place. Thus, we setout to identify the predictive dynamical features of the transitions as well as their first occurrence relative to the closest transition time, through further analyzing of the T_D vector near the transition points. Specifically we utilize measures such as T_M (mean value of all T_D values), variance from the mean of T_D values and variance of dT_D (the spatial derivative of T_D, see figures 3.4 and 3.6) to detect precursors of the transition preceding the bursting onset. As we will show below, we observed systematic changes in these measures prior to the onset of transitions into the bursting. These changes can be interpreted as the early features of incoming transition (or beginnings of the transition itself) and based on that we can obtain lead-time estimate to the in- stance when fully synchronous state takes hold (see methods). We characterize this transition predictability as a function of topologies of both excitatory and inhibitory networks, heterogeneity of cells and noise levels.

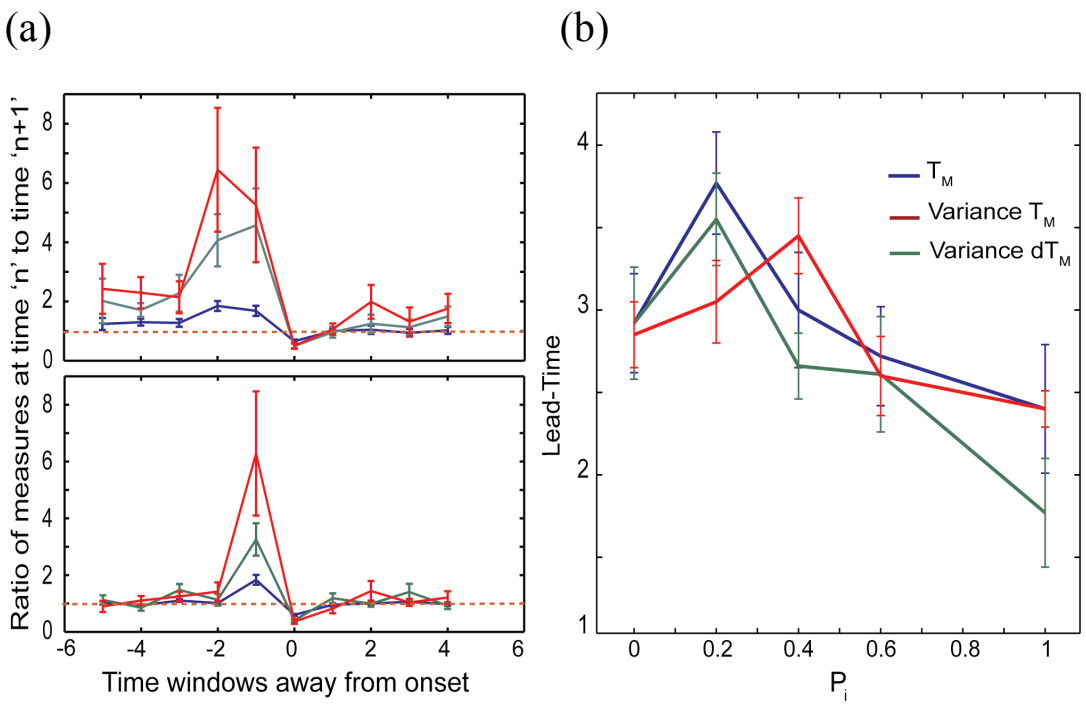

Figure 3.9 The effect of inhibitory connectivity on the lead-time, T_L. (a) the ratio of measures (T_M: blue line, Variance Of T_M: red line, Variance Of dT_M: green line) before and after the onset of the transition into the bursting is shown for P_i=0.2 (top) and P_i=1 (bottom), respectively; P_e=0.15, f_N=0.00005. (b) Based on these ratios, T_L is calculated as a function of the inhibitory connectivity pattern. T_L peaks for P_i=0.2 and then decreases for more random inhibitory topologies.

We want to use measures characterizing properties of T_D to detect precursors of the transitions into the bursting dynamics and calculate the lead-time T_L (or predictability) to the transition, as a time period before the transitions, during which we can detect significant changes in dynamics, as reported by the developed metrics. First, we measure the values of the aforesaid metrics in the time windows immediately preceding the onset of the bursts (as defined by the T_M). We then calculate the ratios of these values obtained in the consecutive time windows. Thus, we calculate $R_N = M_{N+1}/M_N$, where R_N denotes the ratio of the (generalized) measure 'M'

calculated 'N' time-windows before the burst onset (N = 0, 1, 2, 3, 4, 5). We then average the ratios over all the realizations of transitions for given network type.

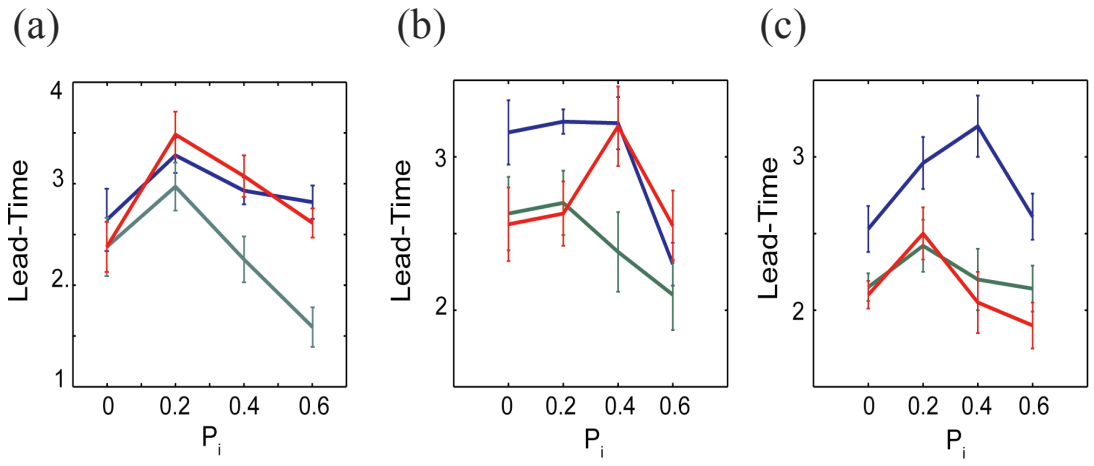

Figure 3.10 T_L varies as a function of inhibitory connectivity (P_i) for excitatory networks with different values of P_e. (a) P_e = 0.0, (b) P_e = 0.15 and (c) P_e = 1.0 where blue, red and green lines are standing for obtained T_L based on the T_M, variance of T_M and variance of dT_M measures respectively.

If the R_N is significantly different from unity we assume that spatial patterning within this time window is persistently and significantly different from that in the prior window. At the same time, the lead-time is defined as the number of time windows prior bursting onset within which the spatio-temporal network pattern undergoes significant change with respect to the one observed in a window before. We defined "predictability" or Lead-time as a number of windows prior to the onset of bursting when the ratio is significantly different from one.

Figure 3.9 depicts estimation of the lead-time as a function of inhibitory

network connectivity. The vertical dashed line (Fig. 3.9a-top and bottom) denotes the transition point into bursting dynamics. We report the ratios of three derivative measures of the T_D vector (T_M, spatial variance of T_D and its spatial derivative, dT_D vector, for given time-window) calculated in the times windows N+1 and N before and after the transition (N=0, 1, 2, 3, 4, 5). Figure 3.9b shows lead-time (T_L). All three measures used show significant changes before the transition to bursting. The changes in variance of both T_D and of dT_D show the largest changes before the transition point. However in terms of estimated lead-time T_M performs somewhat better (see also figures 3.10 and 3.11). The excitatory network topology is fixed (P_e=0.15) and neurons are identical (I_e=1.05) driven by noise (f_N=0.00005). The connectivity pattern of the inhibitory network is being changed from local (P_i=0) to random (P_i=1). The examples of the ratios of the three metrics at the consecutive time-windows are depicted for P_i=0.2 (Fig. 3.9a) and P_i=1 (Fig. 3.9b). We observe that depending on the inhibitory topology all three measures report different predictability intervals—with longer ones being reported for P_i=0.2. Figure 3.9c reports the lead-time as a function of the inhibitory network connectivity. As mentioned before the size of time windows depends on spiking frequency. If we assume that the mean spiking rate is around 10-20Hz the lead-time can be estimated to be up to 200-400ms (4 time-windows). While not a lot, this maybe enough to provide electrical stimulation to disrupt pathological pattern.

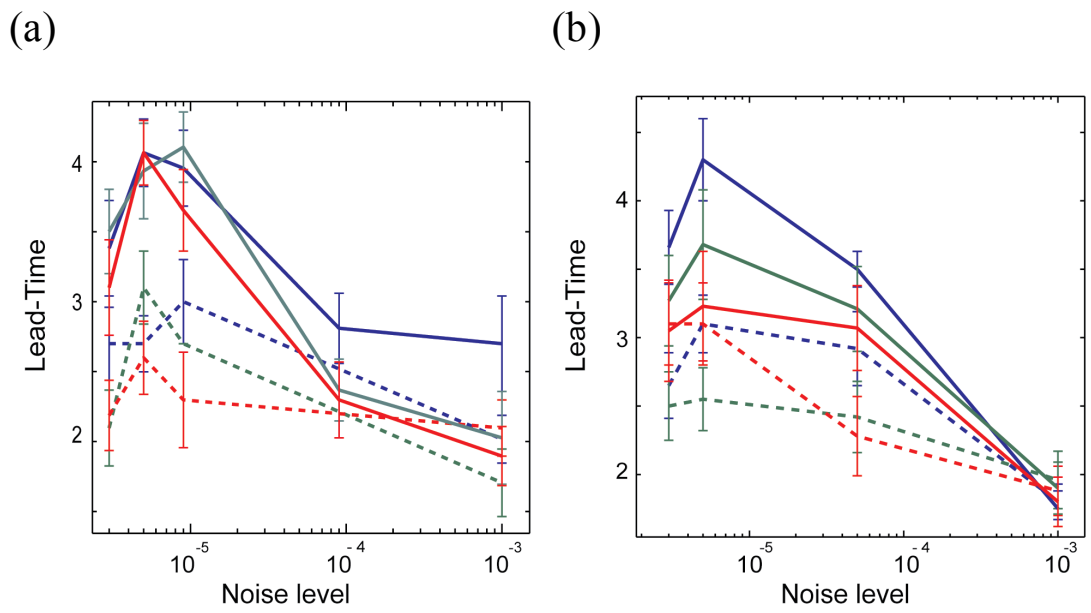

Figure 3.11 The effect of noise on the lead-time of the transitions for both excitatory and interacting excitatory-inhibitory networks. (a) Excitatory networks (P_e=0.15); (b) excitatory and inhibitory networks (P_e=0.15, P_i=0.0). Solid lines denote simulations in which all neurons receive identical external current (I_e=1.05, I_i=0.95), while dashed-lines are representing simulations with distribution of external currents (I_e= 0.95–1.15, I_i =0.9–1.0).

To better understand the interaction of the excitatory and inhibitory topologies on the lead- time (T_L), we explored the effect of inhibition on networks with three excitatory connectivity patterns P_e =0.0, 0.15 and 0.4 having deterministic dynamics (I^e_{exc} =0.95–1.15, I^i_{exc} =0.9–1, Fig. 3.10). Here the general trend is less clear, but there is a moderate decrease of the lead-time for more random inhibitory topologies, with shift of the predictability peak towards values where $P_e \approx P_i$, as reported by T_M.

We next used the measures described above to characterize the effect of noise and variability of neuronal firing frequency on the transition lead-time

for both, the excitatory (Fig. 3.11a) and interacting excitatory-inhibitory (Fig. 3.11b) networks. The solid-lines are for the case when neurons are receiving the same external current, while dashed lines are for the case when the neurons have significantly different intrinsic firing frequencies as their driving current varies between I_e=0.95–1.15 for excitatory cells and I_i =0.9-1.0 for inhibitory cells. Obtained results suggest that predictability is much higher for the networks in which neurons have similar intrinsic firing frequencies, however as expected the lead-time decreases with the increasing noise level.

3.4 Discussion

In this chapter we investigated predictability of network transitions into bursting regime as a function of network structure, cell variability and noise. Initially, we characterized the dynamics for different parameter sets and then we used the developed measures to predict transitions to synchronous activity using spike timings. The networks, as predicted exhibit different types of dynamics, ranging from propagating waves of activity, through coexistence of two phases with short waves of activity and bursting, and finally synchronous dynamics. Addition of inhibition to network shortens the propagating waves, with the transition to bursting suppressed for random inhibitory topologies.

Over the last few decades amount of research is associated with finding robust measures that can detect synchron[109,100,136]. In general these measures require relatively long time series, making them not applicable to measure

relatively rapid transitions in network patterning, such as the onset of seizure. The metrics that we propose here aims to detect instantaneous changes in spatial statistics of spiking coincidence.

The introduced measures centered on analysis of relative spike timings of all firing cells within a given time window. The metrics characterized instantaneous spatial correlations between the cells as a function of their physical distance. The systematic changes in the introduced measures in the time windows preceding the bursting onset were able to predict transition into bursting within few time windows of its onset. It is important to note however that the approach taken does not allow estimating the false positives (i.e. when observed change does not lead to bursting transition), resolving these changes from the ones leading to bursting onset is a subject of ongoing research. The performance of the metrics depended on network topology, noise level and distribution of cellular firing rates. The constructed metrics provide an alternate approach toward gaining an insight on transitions between asynchronous and bursting dynamics. Their advantages are that they can be computed rapidly and thus applied online in clinical use.

CHAPTER IV

Parvalbumin-expressing interneurons drive hippocampal network oscillations and coordinate neuronal communication to facilitate memory consolidation

This chapter is devoted to analysis of the brain activity of mice, which were experimentally recorded in Aton's laboratory. Here, I employ measures to extract the neuronal functional connectivity patterns and its stability upon rapid learning during contextual fear conditioning. The work presented in this chapter was performed in collaboration with Nicolette Ognjanovski, Samantha Schaeffer, Daniel Maruyama, Michal Zochowski, and Sara J. Aton. Nicolette Ognjanovski and Samantha Schaeffer in Aton's laboratory have done all the experimental work presented in this chapter and I employed Functional Clustering Algorithm (previously developed in Zochowski laboratory) and stability measure to analyze this data. *This chapter is part of a manuscript that was submitted to Neuron Journal in October 2015* [89].

4.1 Introduction

Memories can be stored in neural networks by rearranging the network structure through the formation of new connections or varying the efficacy of interactions [137]. These structural changes directly influence the spiking patterns of neurons and introduce heterogeneity in the spatiotemporal patterns of the network. Such heterogeneity in spiking patterns of a network is a reflection of forming new functional connectivity within the network due to new memory storage and consolidation (see figure 4.1a,b).

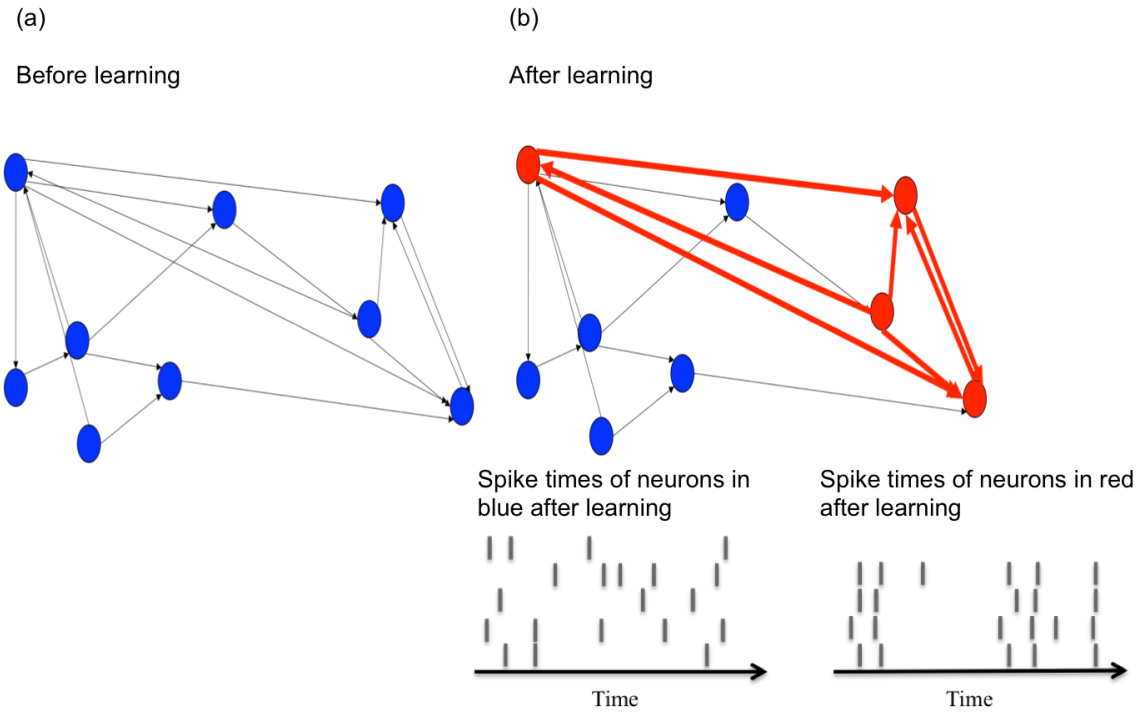

Figure 4.1 Schematic representation of the structural and dynamical reformation due to the learning and memory formation. a) Represent the structure of network before learning and b) Exhibit the structural and dynamical changes due to learning and memory formation. Neurons in red are functionally connected, and their spike timings are very similar.

Therefore developing tools capable of drawing such network-wide

functional connectivity based on the recorded dynamics is vital. Due to the importance of functional connectivity, there have been many measures designed to extract the temporal correlations of recorded time series, for example, cross-correlation and mean phase coherence (MPC). Where cross-correlation defines how closely two signals are changing together and MPC determines the degree of phase locking between the two signals. These measures have a very limited success due to their shortcoming in determining a threshold for the significance of temporal correlations. Here, I employ a functional connectivity method (previously developed in Zochowski lab: Sara Feldt, Daniel Maruyama, Michal zochowski) and extract the functional connectivity based on the statistical correlates of neural firing patterns. Namely, we compute functional connectivity based on the temporal nearness of neurons' spike times - "neurons that wire together fire together" [87]. Based on the temporal evolution of the functional connectivity we introduce a notion of network stability. We use this notion to investigate how memory consolidation changes overall network dynamics and what specific role do the oscillations play in this process.

4.2 Experimental background

Research in Aton lab focuses on understanding the structural and dynamical mechanisms underlying learning and memory consolidation in the hippocampus. There is some evidence indicating that hippocampal oscillations play an important role in reactivation and consolidation of memories following learning[138]. Ognjanovski and Aton suggest that parvalbumin-expressing (PV+) interneurons mediate theta band oscillation

in CA1 and coordinate hippocampal network activity during contextual fear memory (CFM) consolidation. They investigate this hypothesis by employing single-trial training paradigms to examine the effect of PV+ interneurons on the memory consolidation [139]. More specifically, they design contextual fear conditioning (CFC) for mice where animals are transferred into a novel environment and shortly after the replacement they receive a foot shock. This conditioning could result in a long-lasting fear memory (contextual fear memory), with a proper memory consolidation. They record neuronal activities of CA1 area in hippocampus before and after CFC in two groups of animal: a) vehicle-treated mice (DMSO) and b) Mice that were administered the hM4Di ligand clozapine-N-oxide (CNO), which pharmacogenetically inhibits PV+ interneurons. They show that pharmacogenetic inhibition of these neurons immediately following single-trial contextual fear conditioning impairs memory consolidation. Here for DMSO and CNO animals we investigate the recorded spike times before and after CFC. Initially, we compute the Average Minimum Distance (AMD) of populations spike times and from that deduce the functional connectivity. Then we calculate the stability of the functional connectivity for CNO and DMSO groups. Interestingly, in animals that belong to DMSO group, CA1 neuronal functional connectivity patterns become increasingly stable. While in CNO animals, these CFC-induced changes are eliminated by PV+ interneuron inhibition.

4.2.1 Single-neuron recordings

In Aton's laboratory, single-neuron data were discriminated (Offline Sorter;

Plexon) and tracked throughout each experiment. This differentiation was mainly based on the spike waveform, and the relative spike amplitude on the adjacent electrodes [89,86,140]. The analysis was only performed on those neurons that were reliably discriminated, tracked, and continuously recorded during each experiment.

4.2.2 Contextual Fear Conditioning (CFC)

The CFC was performed after 24 h baseline recording, by placing mice into a novel conditioning chamber where they received a small foot shock via the grid floor. A couple of seconds later, each mouse was injected with either clozapine-*N*-oxide (n = 5) dissolved in DMSO or DMSO vehicle alone (vehicle; n = 5). Then mice were transferred to their home cage and remained there for the following 24 h. Next, for assessing the memory consolidation, they were placed into the same conditioning chamber and video monitored (see Fig. 4.2) [86,141]. The increase in the freezing period (comparing to the pre-shock baseline) was quantified as a behavioral measure of memory consolidation [89].

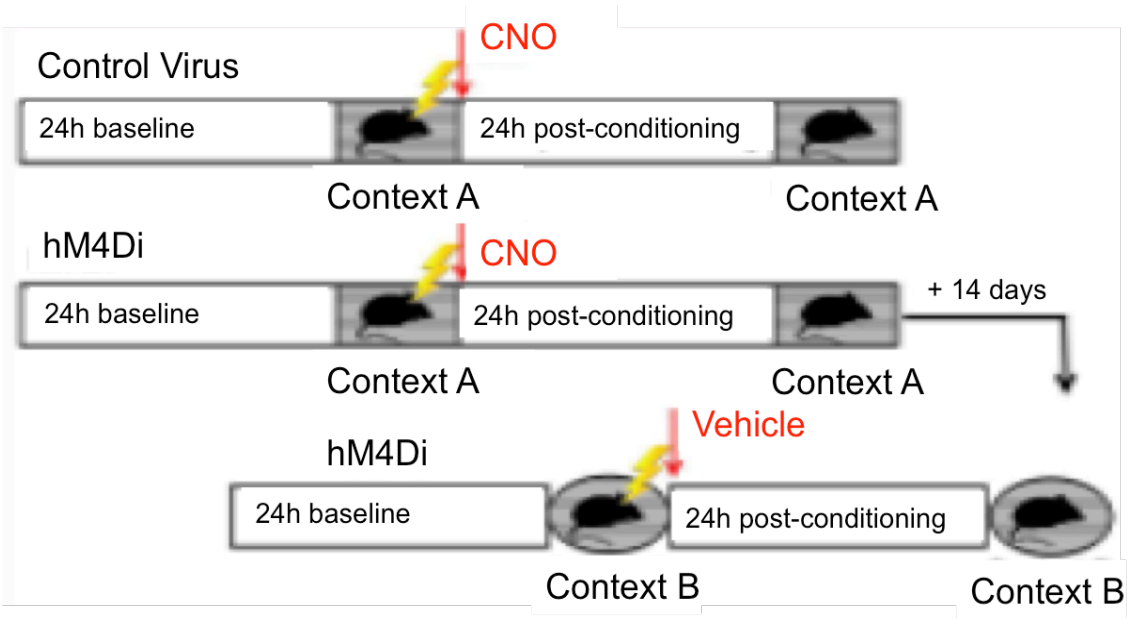

Figure 4.2 Experimental paradigm. The baseline activity of mice is recorded for 24-h in their home cage, and then they were transferred into a novel recording chamber (Context A) for single trial contextual fear conditioning (CFC). After receiving the foot shock, they were administered with CNO and returned to their home cage. Memory consolidation was measured by context-specific freezing that was assessed 24 hours after the CFC. The hM4Di-expressing mice again underwent CFC (after two weeks in a different context, Context B), and next they were administered vehicle (DMSO) [90]. (Image is adapted from Ognjanovski [89])

4.3 Methods

4.3.1 Measures to detect functional connectivity

How to determine the functional connectivity of two neurons? Two neurons are functionally connected, if their spike timings coincide or occur in close temporal proximity from each other. This simple definition is the foundation of developed measures to detect specific correlations within the chaotic network's dynamics. Our laboratory has developed a novel Functional Clustering Algorithm (FCA) that could identify the functional connectivity

within a population of recorded neurons [86]. In this measure similarity between two spike trains is estimated by averaging over the temporal nearness of their spike times, this measure is called 'Average Minimum Distance (AMD)' [142] and can be calculated as follow:

$$AMD_{ij} = \frac{1}{N_i}\sum_k \Delta t_k^i, \quad (4.1)$$

Where 'i' and 'j' correspond to neuron 'i' and 'j' spike trains and Δt^k_{ij} is the least temporal distance between k^{th} spike of neuron 'i' with neuron's j spike times (an example is depicted in Fig. 4.3). This measure gives an estimate of how similar two spike trains are. However, this measure needs a frequency adjustment so that the high frequency spiking would not be mistaken with the high temporal closeness.

To adjust for the frequency effect, an expected AMD distribution is estimated for each pairs of neurons. The significance of the original AMD, from unperturbed spike times, is assessed against this expected AMD value as below:

$$FC_{ij} = \frac{\mu_{j-AMD_{ij}}}{\sigma_j/\sqrt{N_i}} \quad (4.2)$$

Where FC_{ij} stands for the functional connectivity between i and j spike trains, and μ_j, σ_j represent the expected AMD average and its standard deviation.

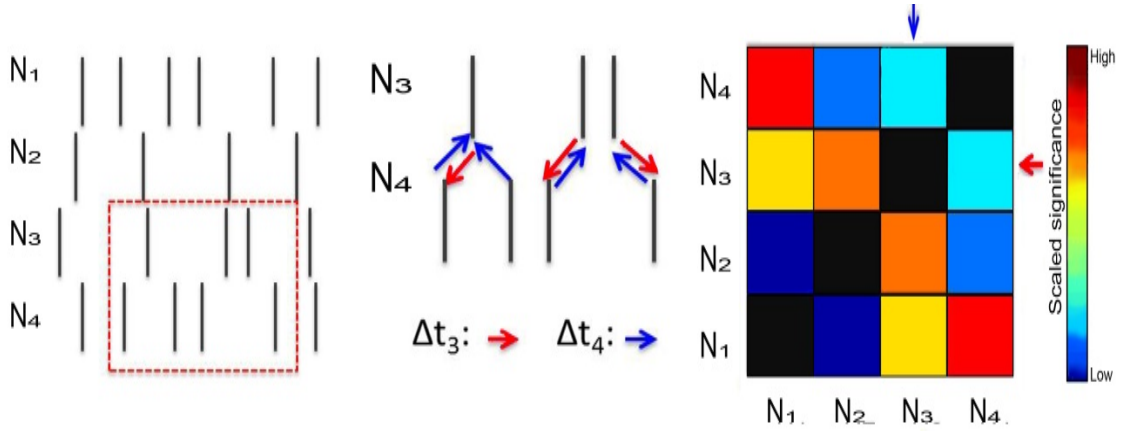

Figure 4.3 Average Minimum Distance measure. Here for four neurons, we calculate the minimum temporal difference between spikes of each pairs of neurons at a specific time-window.

To calculate the average and standard deviation of expected values, (μ_j and σ_j), we take an integral over the sampling minimum distance distribution of neuron's 'j' spike train (S_j) [86].

4.3.2 Stability of functional connectivity

Here we take a rather different approach and instead of focusing on the specific properties of functional connectivity between individual cells we investigated how network-wide functional connectivity evolves with time. This approach can give us a general lead to animal function (learning/ or not learning). Therefore we employ stability measure to see how the network-wide functional connectivity changes over time, is it stable, unstable or follows some specific pattern?

To capture stability of functional connectivity over time, we compute the cosine similarity of the functional connectivity vector at time t and at time t+ Δt, where Δt is our time-window (kept constant, 1minute for all analysis). The cosine similarity measure is one of the simplest ways to calculate the similarity of two signals by computing their inner product space that reflects the cosine of their angle:

$$C_{AB} = \cos\theta_{AB} = \frac{<A,B>}{\sqrt{<A,A>*<B,B>}} \quad (4.6)$$

The result of this cosine similarity is a number between -1 and 1, where 1 represents complete similarity and no change in the network-wide functional connectivity. This similarity measure could also be applied for each time-window against any other time-window to extract possible patterns in network-wide functional connectivity. In figure 4.4, you can see examples of similarity calculations for adjacent data segments, and in figure 4.5 for all to all periods of data.

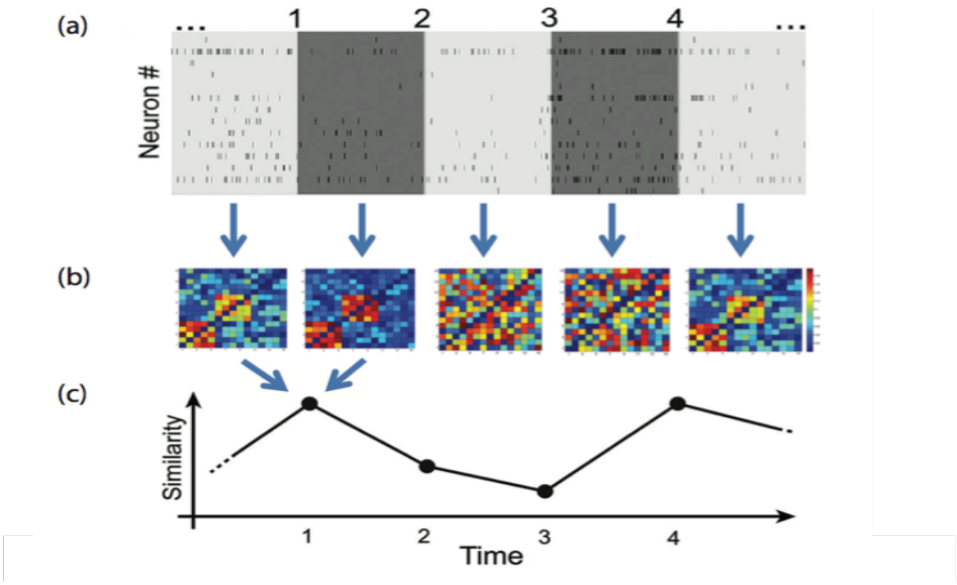

Figure 4.4 Similarity of functional connectivity in consecutive time windows. (Image is adapted from Ognjanovski [86])

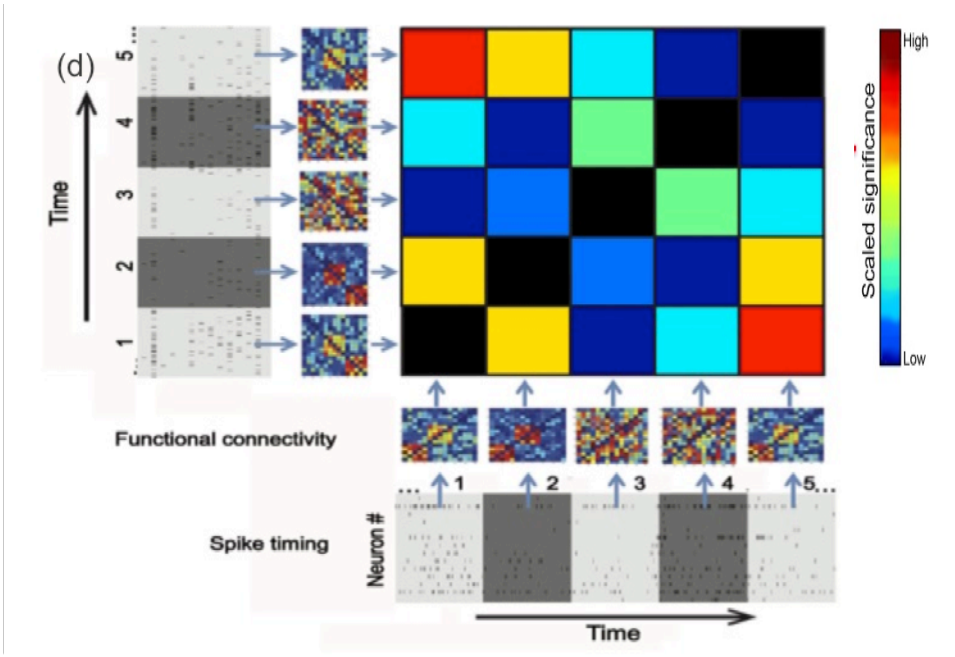

Figure 4.5 Schematic illustration of functional similarity matrix (FSM). Forming FSM matrix using cosine similarity of calculated functional connectivity for each two time-windows.

4.4 Results

Using individual neurons' spike trains, functional connectivity was assessed among the population of stably recorded CA1 neurons (refer to figure 4.2 for the experimental details, and figure 4.3 for calculating functional connectivity). The stability of network-wide functional connectivity was calculated by comparing minute-by-minute network-wide functional connectivity at baseline and following the CFC for both CNO and DMSO animals.

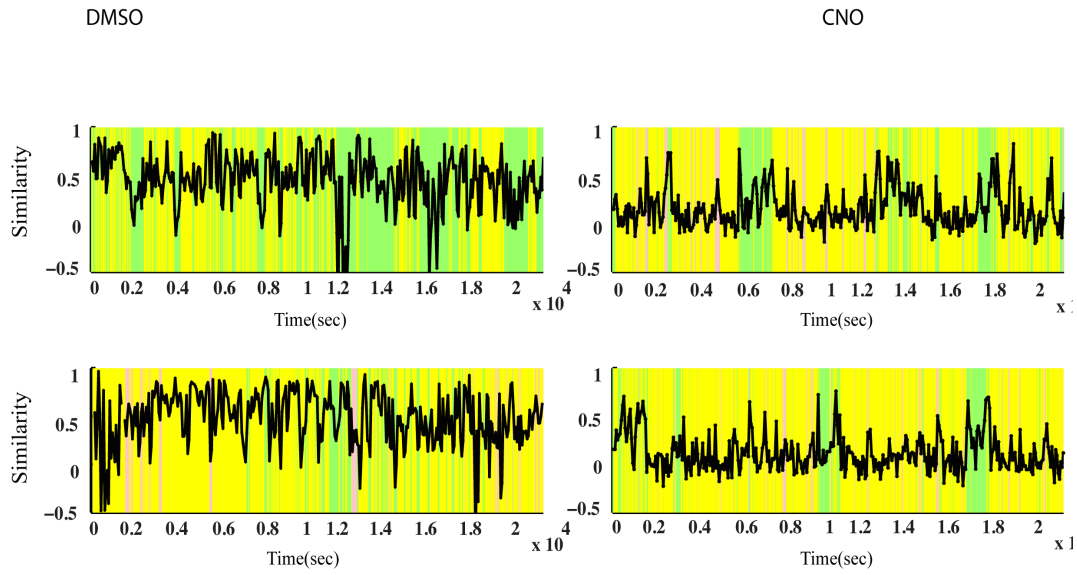

Figure 4.6 The similarity/stability between adjacent data segments. Here we show the stability of functional connectivity for each two adjacent one-minute time windows for DMSO (left column) and CNO (right column) mice prior (top row) and following (bottom row) single-trial contextual fear conditioning (CFC). The background colors denote behavioral states: green denotes wake, pink REM sleep and yellow SWS.

In figure 4.6, we depict the stability of functional connectivity for each two adjacent one-minute time windows for DMSO (Fig. 4.6 left column) and CNO (Fig. 4.6 right column) mice prior (Fig. 4.6 top row) and following (Fig. 4.6 bottom row) single-trial contextual fear conditioning (CFC). Here colors reflect different sleep phases; green for wake, pink for rapid eye movement sleep (REM) and yellow for slow-wave sleep (SWS). In vehicle-treated mice, the average of the CA1 network stability was enhanced following CFC; this stabilization was present in both post-CFC NREM sleep and wake, and was blocked by PV+ interneuron inhibition in CNO. Statistical significance of this progressive increase in stability is depicted in figure 4.7 that matches properly with the freezing behavior of the animal.

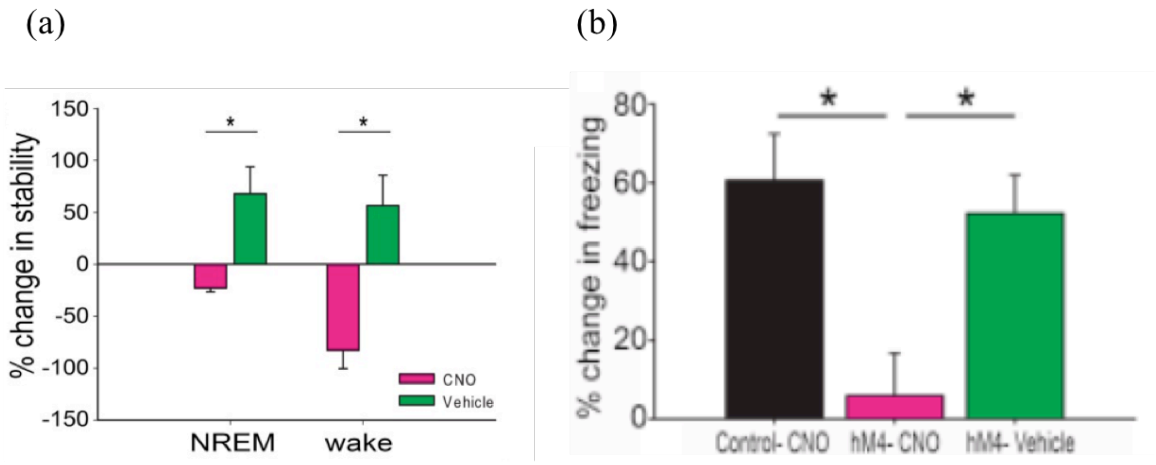

Figure 4.7 Change in stability following CFC. a) The mean minute-to-minute CA1 network stability increases during both NREM and wake. b) Memory consolidation was assessed based on the freezing behavior of animal. Here we can clearly see the inhibition of PV+ interneurons interferes with learning and memory consolidation (Image is adapted from Ognjanovski [89])

In figure 4.8 we depict the functional similarity matrix (FSM), which represents the patterns of the similarity of the network-wide functional connectivity at each time point (one-minute time window) with any other time window. This FSM shows how the stability of functional connectivity in CA1 networks evolves with time. In figure 4.8 FSMs of a control and hM4Di-expressing mouse at baseline, and over the first six h post-CFC (vehicle and CNO conditions) is shown. Color in the body denotes the degree of similarity between functional connectivity of any given two time points in the recording. The formed temporal patterns in the FSM might convey information regarding animal's function. For example in the CNO case in baseline when the animal is awake we see repetitive patterns of high stability (periods of higher intensity colors), these repetitive similarities to some extent stay intact after CFC and CNO injection but weakened. These

repetitive patterns might be associated with a specific task or location in the cage. However, the CNO animal does not show any particular temporal pattern in SWS state (their stability scores are not significant). In the case of animal treated with DMSO, we could clearly see the formation of episodes of high stability regions (shown with higher intensity colors) associated with SWS sleep postconditioning. We can see that there is a reoccurring pattern of high stability episodes over time especially during SWS state. This repetition could be associated with retrieving the fear memory that is successfully stored in DMSO animals and manifest itself by a high degree of similarity/stability in network-wide firing pattern. This reoccurrence of high similarity events during SWS, postconditioning, are explicit for DMSO animals where the behavioral scores also show successful learning and memory consolidation.

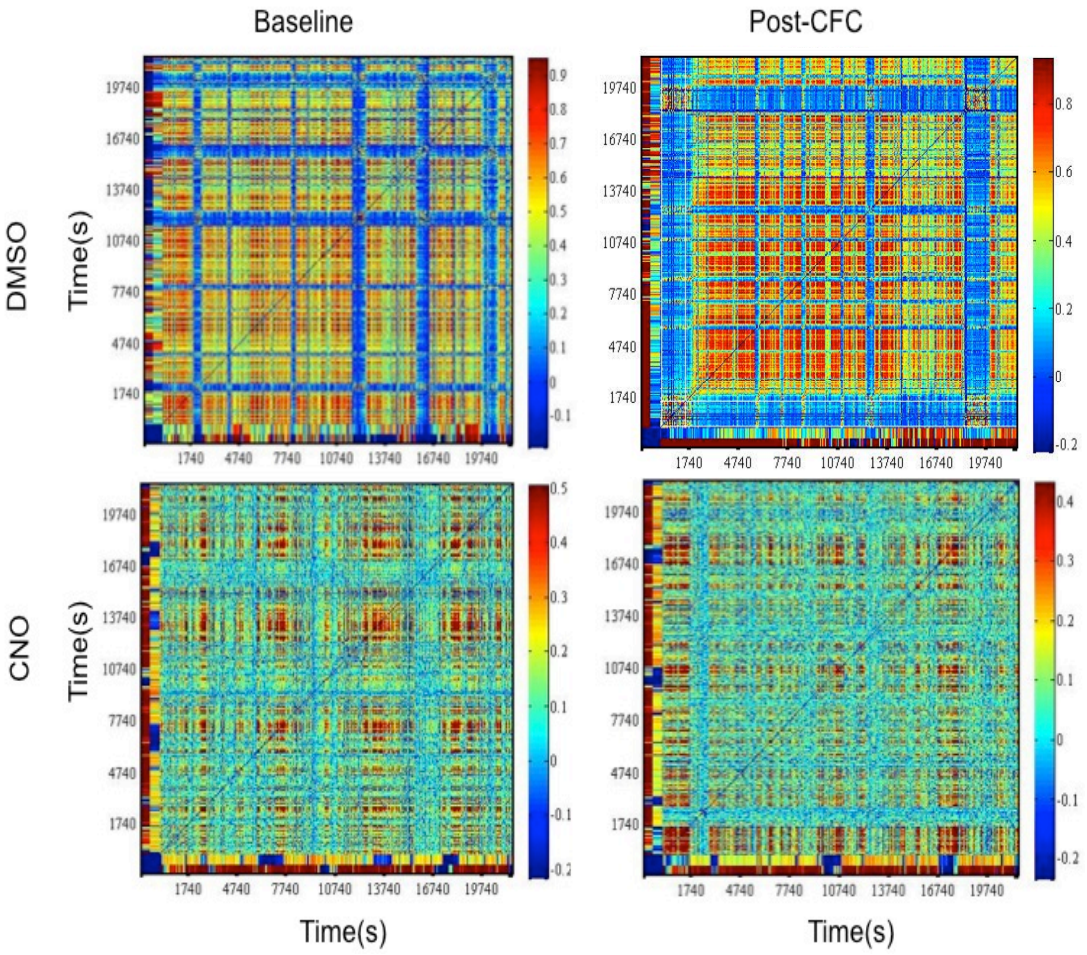

Figure 4.8 Functional Similarity Matrix (FSM). The FSM displays the similarity of functional connectivity patterns across time. Here we illustrated the CA1 network FSMs for DMSO and CNO animal at baseline, and over the first 6 h post-CFC. Where the degree of similarity between functional connectivity patterns at any given time point with all other time points is represented with a color. The two outermost color bars represent the behavioral state of the animal (outer, blue - wake, red – NREM and REM) and the relative firing frequency (inner, blue - low, red - high).

4.5 Discussion

In this chapter, I analyzed the data taken from Aton' lab and investigate the role of PV+ interneurons in learning and memory consolidation by analyzing the spatiotemporal patterns of neuronal network of CA1 area. To analyze the

data, the similarity between two spike trains is measured by averaging over temporal nearness of their spike times; this measure is called Average Minimum Distance (AMD). Pairwise AMD values were calculated based on spike trains from the entire population of stably recorded neurons in each mouse. From these values, a functional connectivity matrix is generated, which represents the pattern of functional connectivity at any time point. Pairs with smaller AMD values are more likely to be functionally connected. We compute the stability of the functional connectivity over time for two distinct groups of animals, DMSO (vehicle) and CNO (animals that were administrated the hM4Di ligand clozapine-N-oxide that inhibits the activity of PV + interneurons).

Our collaborators in Aton's lab assessed the memory consolidation in animals by behavioral tests, and showed that in CNO animals this memory consolidation was disrupted. Interestingly, we could show that stability of calculated functional connectivity increases in the normal CFC and decreases in case of CNO animals. This result suggests that PV+ interneurons activity is essential for memory consolidation in agreement with our collaborators findings in Aton's lab.

CHAPTER V

Summary and conclusions

The brain is the most complex biological structure, made of hundred billions of tightly interconnected neurons. The incredible computational power and degree of complexity involved in the brain structure and function is the biggest mystery of the modern time. Its roots can be traced back to the mutual interactions of neurons that construct this entangled network. The focus of this dissertation is to shed light on how the interactions among these entities lead to the different dynamics and eventually determine the brain function.

In Chapter II, I studied the structural foundation of the different brain's dynamical modes of activities based on the interplay between cellular properties and network coupling characteristics. More specifically, I identified conditions that promote synchrony in mixed networks of Type I and Type II neurons under varying network connectivity distributions. The obtained results indicate that not only overall connectivity topology in the networks matters but also statistical distributions of cell connectivity properties, I showed that relatively few highly rewired Type II cells can significantly increase the level of network-wide synchrony, however, this

degree of synchrony is not realized when these highly rewired cells have Type I excitability. I also showed that establishing specifically connected cliques might cause the emergence of globally synchronized activity depending on the excitability type of these neurons. This result could have significant implications when characterizing real-world network connectivity patterns, where statistic of cell connectivity is usually limited to only a few identified cells, as we showed that relatively few cells of specific dynamical and connectivity properties could significantly change spatiotemporal patterning.

In chapter III, I took a step further and developed a set of measures to quantify and predict spontaneous network transitions from asynchronous dynamics to the synchronous dynamics. These spontaneous transitions into the synchronous activity of the network may correspond changes of neural activity at the onset of epileptic seizures. Namely, I investigated whether and under what conditions we could identify and later detect early dynamical signs of transitions from asynchronous to synchronous dynamics in a highly simplified setting. Our developed measures are capable of capturing early spatial features of network reorganization upon impending transition into bursting dynamics. These results may be important for the development of improved techniques for detection of seizure onset in clinical devices.

Following the study of structural foundations in shaping different modes of dynamics in chapter II and developing measures to predict spontaneous transitions from one to another in chapter III, in chapter IV, I explored dynamical network changes associated with memory consolidation. Specifically, I analyze in vivo experimental data obtained from Aton laboratory to show that increase of stability of functional network

representation predicts successful memory consolidation. Further, both the increase stability and behavioral performance are linked to the presence of theta band oscillations indicating that these could play a central role in the dynamics of memory consolidation.

In summary, this dissertation highlights the importance of understanding neuronal structure and dynamics to elucidate the brain function. We developed and employed computational and statistical tools to detect emerging patterns and correlations in network dynamics in both simplified simulated networks and experimentally recorded data.

Today with all the advances in spectroscopy, imaging and electrophysiology recordings we are experiencing an explosion in producing experimental data - data, that ten years ago we would not dream of. Thus, it is crucial to develop analytical tools and measures that can quantify experimental data, shed light on the hidden patterns and allow building predictive theories of the brain function. This dissertation provides one of many needed building blocks in this direction.

BIBLIOGRAPHY

1. Gil, V., Nocentini, S. & Del Río, J. a. Historical first descriptions of Cajal-Retzius cells: from pioneer studies to current knowledge. *Front. Neuroanat.* **8,** 32 (2014).
2. López-Muñoz, F., Boya, J. & Alamo, C. Neuron theory, the cornerstone of neuroscience, on the centenary of the Nobel Prize award to Santiago Ramón y Cajal. *Brain Res. Bull.* **70,** 391–405 (2006).
3. Finger, S. *Origins of Neuroscience BT - A History of Explorations Into Brain Function*. *A History of Explorations Into Brain Function* (2001). doi:10.1002/ana.410360532
4. Kandel, E. R., Schwartz, J. H. & Jessell, T. M. *Principles of Neural Science*. *Neurology* **3,** (2000).
5. Buzsáki, G. *Rhythms of the Brain*. (2006). doi:10.1093/acprof:oso/9780195301069.001.0001
6. Sejnowski, T. J., Koch, C. & Churchland, P. S. Computational neuroscience. *Science (80-.).* **241,** 1299–1306 (1988).
7. Abbott, L. F. Lapicque's introduction of the integrate-and-fire model neuron (1907). *Brain Res. Bull.* **50,** 303–304 (1999).
8. Brunel, N. & Van Rossum, M. C. W. Lapicque's 1907 paper: From frogs to integrate-and-fire. *Biol. Cybern.* **97,** 337–339 (2007).
9. Hodgkin, A. L. & Huxley, A. F. Quantitative description of nerve current - E. *J. Physiol.* **117,** 500–544 (1952).
10. Bullock, T. H. *et al.* Neuroscience. The neuron doctrine, redux. *Science (80-.).* **310,** 791–793 (2005).
11. Pelvig, D. P., Pakkenberg, H., Stark, a. K. & Pakkenberg, B. Neocortical glial cell numbers in human brains. *Neurobiol. Aging* **29,** 1754–1762 (2008).

12. Bear, M. F., Connors, B. W. & Paradiso, M. A. *Neuroscience: Exploring the brain (3rd ed.). Neuroscience: Exploring the brain (3rd ed.)*. (2007). at <http://www.mendeley.com/catalog/neuroscience-exploring-brain-3rd-ed/>

13. Borg-Graham, L. J. Biophysics of Computation: Information processing in single neurons by Christof Koch. *Trends Neurosci.* **22,** 328–329 (1999).

14. Action potential. at <https://psychlopedia.wikispaces.com/resting+potential>

15. Lee, S. H. & Dan, Y. Neuromodulation of brain states. *Neuron* **76,** 109–222 (2012).

16. Sarter, M. & Bruno, J. P. Cognitive functions of cortical acetylcholine: toward a unifying hypothesis. *Brain Res. Rev.* **23,** 28–46 (1997).

17. Parikh, V. & Sarter, M. Cholinergic mediation of attention: Contributions of phasic and tonic increases in prefrontal cholinergic activity. *Ann. N. Y. Acad. Sci.* **1129,** 225–235 (2008).

18. Sarter, M., Hasselmo, M. E., Bruno, J. P. & Givens, B. Unraveling the attentional functions of cortical cholinergic inputs: Interactions between signal-driven and cognitive modulation of signal detection. *Brain Res. Rev.* **48,** 98–111 (2005).

19. Money, K. M. & Stanwood, G. D. Developmental origins of brain disorders: roles for dopamine. *Front. Cell. Neurosci.* **7,** 260 (2013).

20. Eppinger, B., Hämmerer, D. & Li, S.-C. Neuromodulation of reward-based learning and decision making in human aging. *Ann. N. Y. Acad. Sci.* **1235,** 1–17 (2011).

21. Remy, P., Doder, M., Lees, A., Turjanski, N. & Brooks, D. Depression in Parkinson's disease: Loss of dopamine and noradrenaline innervation in the limbic system. *Brain* **128,** 1314–1322 (2005).

22. Chaudhuri, K. R. & Schapira, A. H. Non-motor symptoms of Parkinson's disease: dopaminergic pathophysiology and treatment. *Lancet Neurol.* **8,** 464–474 (2009).

23. Izhikevich, E. M. *Dynamical Systems in Neuroscience*. *Dynamical Systems* (2007). doi:10.1017/S0143385704000173

24. Fink, C. G., Booth, V. & Zochowski, M. Cellularly-driven differences in network synchronization propensity are differentially modulated by

firing frequency. *PLoS Comput. Biol.* **7,** 1–14 (2011).

25. Ermentrout, G. B. Type I Membranes, Phase Resetting Curves, and Synchrony. *Neural Comput.* **8,** 979–1001 (1996).

26. Rinzel, J. & Ermentrout, G. B. in *Methods in neuronal modeling* 251–292 (1989). at <http://mitpress.mit.edu/books/methods-neuronal-modeling>

27. Gutkin, B. S., Ermentrout, G. B. & Reyes, A. D. Phase-response curves give the responses of neurons to transient inputs. *J. Neurophysiol.* **94,** 1623–1635 (2005).

28. Stiefel, K. M., Gutkin, B. S. & Sejnowski, T. J. Cholinergic neuromodulation changes phase response curve shape and type in cortical pyramidal neurons. *PLoS One* **3,** e3947 (2008).

29. Boundless. Signal Summation. (2015). at <https://www.boundless.com/biology/textbooks/boundless-biology-textbook/the-nervous-system-35/how-neurons-communicate-200/signal-summation-764-11997/images/fig-ch35_02_08/>

30. Gershenson, C. A General Methodology for Designing Self-Organizing Systems. *Arxiv Prepr. nlin0505009* **V,** 1–28 (2005).

31. Heylighen, F. Self-organization, emergence and the architecture of complexity. *Complexity* **18,** 23–32 (1989).

32. Hebb, D. O. *The organization of behavior: a neuropsychological theory*. *Science Education* **44,** (1949).

33. Bi, G. Q. & Poo, M. M. Synaptic modifications in cultured hippocampal neurons: dependence on spike timing, synaptic strength, and postsynaptic cell type. *J. Neurosci.* **18,** 10464–10472 (1998).

34. BRAIN INITIATIVE. at <http://braininitiative.nih.gov/>

35. Human Connectome Project . at <http://www.humanconnectomeproject.org/about/>

36. Chung, K. *et al.* Structural and molecular interrogation of intact biological systems. *Nature* **497,** 332–7 (2013).

37. van den Heuvel, M. P. & Hulshoff Pol, H. E. Exploring the brain network: a review on resting-state fMRI functional connectivity. *Eur. Neuropsychopharmacol.* **20,** 519–34 (2010).

38. Blatow, M., Nennig, E., Durst, A., Sartor, K. & Stippich, C. fMRI

reflects functional connectivity of human somatosensory cortex. *Neuroimage* **37,** 927–936 (2007).

39. Ferreri, F. *et al.* Human brain connectivity during single and paired pulse transcranial magnetic stimulation. *Neuroimage* **54,** 90–102 (2011).

40. Britz, J., Van De Ville, D. & Michel, C. M. BOLD correlates of EEG topography reveal rapid resting-state network dynamics. *Neuroimage* **52,** 1162–1170 (2010).

41. Sporns, O. Graph theory methods for the analysis of neural connectivity patterns. *Neurosci. databases A Pract. Guid.* 169–183 (2002). doi:10.1007/978-1-4615-1079-6_12

42. Felleman, D. J. & Van Essen, D. C. Distributed hierarchical processing in the primate cerebral cortex. *Cereb. Cortex* **1,** 1–47 (1991).

43. Mesulam, M. M. From sensation to cognition. *Brain* **121 (Pt 6,** 1013–52 (1998).

44. Sepulcre, J. *et al.* The organization of local and distant functional connectivity in the human brain. *PLoS Comput. Biol.* **6,** 1–15 (2010).

45. Watts, D. & Strogatz, S. Collective dynamics of 'small-world'networks. *Nature* **393,** 440–442 (1998).

46. Hilgetag, C. C., Burns, G. a, O'Neill, M. a, Scannell, J. W. & Young, M. P. Anatomical connectivity defines the organization of clusters of cortical areas in the macaque monkey and the cat. *Philos. Trans. R. Soc. Lond. B. Biol. Sci.* **355,** 91–110 (2000).

47. Boccaletti, S., Latora, V., Moreno, Y., Chavez, M. & Hwang, D.-U. Complex networks: Structure and dynamics. *Phys. Rep.* **424,** 175–308 (2006).

48. Sporns, O. & Zwi, J. D. The small world of the cerebral cortex. *Neuroinformatics* **2,** 145–162 (2004).

49. Barabási, A.-L. & Albert, R. Emergence of scaling in random networks. *Science (80-.).* **286,** 509–512 (1999).

50. Beggs, J. M. & Plenz, D. Neuronal Avalanches in Neocortical Circuits. *J. Neurosci.* **23,** 11167–11177 (2003).

51. Bonifazi, P. *et al.* GABAergic hub neurons orchestrate synchrony in developing hippocampal networks. *Science (80-.).* **326,** 1419–24

(2009).

52. Crossley, N. a *et al.* Cognitive relevance of the community structure of the human brain functional coactivation network. *Proc. Natl. Acad. Sci. U. S. A.* **110,** 11583–8 (2013).

53. van den Heuvel, M. P. & Sporns, O. Rich-Club Organization of the Human Connectome. *J. Neurosci.* **31,** 15775–15786 (2011).

54. Towlson, E. K., Vértes, P. E., Ahnert, S. E., Schafer, W. R. & Bullmore, E. T. The rich club of the C. elegans neuronal connectome. *J. Neurosci.* **33,** 6380–7 (2013).

55. van den Heuvel, M. P., Kahn, R. S., Goñi, J. & Sporns, O. High-cost, high-capacity backbone for global brain communication. *Proc. Natl. Acad. Sci. U. S. A.* **109,** 11372–7 (2012).

56. de Reus, M. a & van den Heuvel, M. P. Rich club organization and intermodule communication in the cat connectome. *J. Neurosci.* **33,** 12929–39 (2013).

57. Box 3 : The economy of brain network organization : Nature Reviews Neuroscience. at <http://www.nature.com/nrn/journal/v13/n5/box/nrn3214_BX3.html>

58. Butts, D. a *et al.* Temporal precision in the neural code and the timescales of natural vision. *Nature* **449,** 92–95 (2007).

59. Dayan, P. & Abbott, L. F. Theoretical Neuroscience: Computational and Mathematical Modeling of Neural Systems. *Comput. Math. Model. Neural ...* 480 (2001). doi:10.1016/j.neuron.2008.10.019

60. Llinás, R. & Yarom, Y. Oscillatory properties of guinea-pig inferior olivary neurones and their pharmacological modulation: an in vitro study. *J. Physiol.* **376,** 163–182 (1986).

61. Steriade, M., Gloor, P., Llinás, R. R., Lopes de Silva, F. H. & Mesulam, M. M. Report of IFCN Committee on Basic Mechanisms. Basic mechanisms of cerebral rhythmic activities. *Electroencephalogr. Clin. Neurophysiol.* **76,** 481–508 (1990).

62. Fries, P. A mechanism for cognitive dynamics: neuronal communication through neuronal coherence. *Trends Cogn. Sci.* **9,** 474–80 (2005).

63. Fell, J. & Axmacher, N. The role of phase synchronization in memory processes. *Nat. Rev. Neurosci.* **12,** 105–118 (2011).

64. Schnitzler, A. & Gross, J. Normal and pathological oscillatory communication in the brain. *Nat. Rev. Neurosci.* **6,** 285–296 (2005).

65. Fries, P. Neuronal gamma-band synchronization as a fundamental process in cortical computation. *Annu. Rev. Neurosci.* **32,** 209–224 (2009).

66. Gregoriou, G. G., Gotts, S. J., Zhou, H. & Desimone, R. High-frequency, long-range coupling between prefrontal and visual cortex during attention. *Science* **324,** 1207–1210 (2009).

67. Müller, M. M. *et al.* Visually induced gamma-band responses in human electroencephalographic activity--a link to animal studies. *Exp. Brain Res.* **112,** 96–102 (1996).

68. Tallon-Baudry, C., Bertrand, O., Delpuech, C. & Pernier, J. Stimulus specificity of phase-locked and non-phase-locked 40 Hz visual responses in human. *J. Neurosci.* **16,** 4240–4249 (1996).

69. Tallon-Baudry, C., Bertrand, O., Delpuech, C. & Permier, J. Oscillatory gamma-band (30-70 Hz) activity induced by a visual search task in humans. *J. Neurosci.* **17,** 722–734 (1997).

70. Gruber, T., Müller, M. M. & Keil, A. Modulation of induced gamma band responses in a perceptual learning task in the human EEG. *J. Cogn. Neurosci.* **14,** 732–744 (2002).

71. Lee, H., Simpson, G. V, Logothetis, N. K. & Rainer, G. Phase locking of single neuron activity to theta oscillations during working memory in monkey extrastriate visual cortex. *Neuron* **45,** 147–156 (2005).

72. Kahana, M. J., Sekuler, R., Caplan, J. B., Kirschen, M. & Madsen, J. R. Human theta oscillations exhibit task dependence during virtual maze navigation. *Nature* **399,** 781–784 (1999).

73. Raghavachari, S. *et al.* Gating of human theta oscillations by a working memory task. *J. Neurosci.* **21,** 3175–3183 (2001).

74. Jones, M. W. & Wilson, M. a. Theta rhythms coordinate hippocampal-prefrontal interactions in a spatial memory task. *PLoS Biol.* **3,** 1–13 (2005).

75. Varela, F., Lachaux, J. P., Rodriguez, E. & Martinerie, J. The brainweb: phase synchronization and large-scale integration. *Nat. Rev. Neurosci.* **2,** 229–239 (2001).

76. Rutishauser, U., Ross, I. B., Mamelak, A. N. & Schuman, E. M.

Human memory strength is predicted by theta-frequency phase-locking of single neurons. *Nature* **464,** 903–907 (2010).

77. Uhlhaas, P. J. & Singer, W. Neural Synchrony in Brain Disorders: Relevance for Cognitive Dysfunctions and Pathophysiology. *Neuron* **52,** 155–168 (2006).

78. Schwab, B. C. *et al.* Synchrony in Parkinson's disease: importance of intrinsic properties of the external globus pallidus. *Front. Syst. Neurosci.* **7,** 1–7 (2013).

79. Fisher, R. S. *et al.* Epileptic seizures and epilepsy: Definitions proposed by the International League Against Epilepsy (ILAE) and the International Bureau for Epilepsy (IBE). *Epilepsia* **46,** 470–472 (2005).

80. Jiruska, P. *et al.* High-frequency network activity, global increase in neuronal activity, and synchrony expansion precede epileptic seizures in vitro. *J. Neurosci.* **30,** 5690–5701 (2010).

81. Jiruska, P. *et al.* Synchronization and desynchronization in epilepsy: controversies and hypotheses. *J. Physiol.* **591,** 787–97 (2013).

82. Rampp, S. & Stefan, H. Fast activity as a surrogate marker of epileptic network function? *Clin. Neurophysiol.* **117,** 2111–7 (2006).

83. Smart, O. *et al.* Mapping and mining interictal pathological gamma (30-100 Hz) oscillations with clinical intracranial EEG in patients with epilepsy. *Expert Syst. Appl.* **39,** 7355–7370 (2012).

84. Mofakham, S. & Zochowski, M. Measuring predictability of autonomous network transitions into bursting dynamics. *BMC Neurosci.* **15,** P2 (2014).

85. Feldt, S. *et al.* Functional clustering in hippocampal cultures: relating network structure and dynamics. *Phys. Biol.* **7,** 046004 (2010).

86. Ognjanovski, N., Maruyama, D., Lashner, N., Zochowski, M. & Aton, S. J. CA1 hippocampal network activity changes during sleep-dependent memory consolidation. *Front. Syst. Neurosci.* **8,** 61 (2014).

87. Doidge, N. The Brain That Changes Itself: Stories of Personal Triumph from the Frontiers of Brain Science. *Brain* 448 (2007). doi:10.1097/NMD.0b013e31817d2a8d

88. Mofakham, S. & Zochowski, M. Measuring predictability of autonomous network transitions into bursting dynamics. *PLoS One* **10,**

e0122225 (2015).

89. Ognjanovski N, Schaeffer S, Mofakham S, Maruyama D, Zochowski M, A. S. Hippocampal memory consolidation and state-dependent network oscillations are coordinated by parvalbumin-expressing interneuron networks. *Neuron*

90. Steinmetz, P. N. *et al.* Attention modulates synchronized neuronal firing in primate somatosensory cortex. *Nature* **404,** 187–190 (2000).

91. Fries, P., Reynolds, J. H., Rorie, a E. & Desimone, R. Modulation of oscillatory neuronal synchronization by selective visual attention. *Science* **291,** 1560–1563 (2001).

92. Fell, J. *et al.* Human memory formation is accompanied by rhinal-hippocampal coupling and decoupling. *Nat. Neurosci.* **4,** 1259–1264 (2001).

93. Goldberg, J. A., Rokni, U., Boraud, T., Vaadia, E. & Bergman, H. Spike Synchronization in the Cortex-Basal Ganglia Networks of Parkinsonian Primates Reflects Global Dynamics of the Local Field Potentials. *J Neurosci* **24,** 6003–6010 (2004).

94. Wichmann, T., Delong, M. R., Guridi, J. & Obeso, J. a. Milestones in research on the pathophysiology of Parkinson's disease. *Mov. Disord.* **26,** 1032–1041 (2011).

95. Uhlhaas, P. J. & Singer, W. Abnormal neural oscillations and synchrony in schizophrenia. *Nat. Rev. Neurosci.* **11,** 100–113 (2010).

96. Watts, D. J. & Strogatz, S. H. Collective dynamics of 'small-world' networks. *Nature* **393,** 440–442 (1998).

97. Leone, M. J. *et al.* Synchronization properties of heterogeneous neuronal networks with mixed excitability type. *Phys. Rev. E* **91,** 1–7 (2015).

98. Stiefel, K. M., Gutkin, B. S. & Sejnowski, T. J. The effects of cholinergic neuromodulation on neuronal phase-response curves of modeled cortical neurons. *J. Comput. Neurosci.* **26,** 289–301 (2009).

99. Golomb, D. & Rinzel, J. Dynamics of globally coupled inhibitory neurons with heterogeneity. *Phys. Rev. E* **48,** 4810–4814 (1993).

100. Golomb, D. & Rinzel, J. Clustering in globally coupled inhibitory neurons. *Phys. D Nonlinear Phenom.* **72,** 259–282 (1994).

101. Dyhrfjeld-Johnsen, J. *et al.* Topological determinants of epileptogenesis in large-scale structural and functional models of the dentate gyrus derived from experimental data. *J. Neurophysiol.* **97,** 1566–1587 (2007).

102. Buckmaster, P. S. & Jongen-Rêlo, a L. Highly specific neuron loss preserves lateral inhibitory circuits in the dentate gyrus of kainate-induced epileptic rats. *J. Neurosci.* **19,** 9519–9529 (1999).

103. Santhakumar, V., Aradi, I. & Soltesz, I. Role of mossy fiber sprouting and mossy cell loss in hyperexcitability: a network model of the dentate gyrus incorporating cell types and axonal topography. *J. Neurophysiol.* **93,** 437–53 (2005).

104. Morgan, R. J. & Soltesz, I. Nonrandom connectivity of the epileptic dentate gyrus predicts a major role for neuronal hubs in seizures. *Proc. Natl. Acad. Sci.* **105,** 6179–6184 (2008).

105. Lopes da Silva, F. *et al.* Epilepsies as dynamical diseases of brain systems: basic models of the transition between normal and epileptic activity. *Epilepsia* **44 Suppl 1,** 72–83 (2003).

106. Lopes da Silva, F. H. *et al.* Dynamical diseases of brain systems: different routes to epileptic seizures. *IEEE Trans. Biomed. Eng.* **50,** 540–548 (2003).

107. Lehnertz, K. & Elger, C. E. Can epileptic seizures be predicted? Evidence from nonlinear time series analysis of brain electrical activity. *Phys Rev Lett* **80,** 5019–5022 (1998).

108. Mormann, F. *et al.* On the predictability of epileptic seizures. *Clin. Neurophysiol.* **116,** 569–587 (2005).

109. Mormann, F., Lehnertz, K., David, P. & E. Elger, C. Mean phase coherence as a measure for phase synchronization and its application to the EEG of epilepsy patients. *Phys. D Nonlinear Phenom.* **144,** 358–369 (2000).

110. Le Van Quyen, M. *et al.* Anticipation of epileptic seizures from standard EEG recordings. *Lancet* **357,** 183–188 (2001).

111. Mormann, F., Andrzejak, R. G., Elger, C. E. & Lehnertz, K. Seizure prediction: the long and winding road. *Brain* **130,** 314–333 (2007).

112. Andrzejak, R. *et al.* Testing the null hypothesis of the nonexistence of a preseizure state. *Phys. Rev. E* **67,** 010901 (2003).

113. Chaovalitwongse, W. *et al.* Performance of a seizure warning algorithm based on the dynamics of intracranial EEG. *Epilepsy Res.* **64,** 93–113 (2005).

114. Aschenbrenner-Scheibe, R. *et al.* How well can epileptic seizures be predicted? An evaluation of a nonlinear method. *Brain* **126,** 2616–26 (2003).

115. Truccolo, W. *et al.* Single-neuron dynamics in human focal epilepsy. *Nat. Neurosci.* **14,** 635–641 (2011).

116. Babb, T. L., Wilson, C. L. & Isokawa-Akesson, M. Firing patterns of human limbic neurons during stereoencephalography (SEEG) and clinical temporal lobe seizures. *Electroencephalogr. Clin. Neurophysiol.* **66,** 467–82 (1987).

117. Engel, A. K., Moll, C. K. E., Fried, I. & Ojemann, G. a. Invasive recordings from the human brain: clinical insights and beyond. *Nat. Rev. Neurosci.* **6,** 35–47 (2005).

118. Ziburkus, J., Cressman, J. R., Barreto, E. & Schiff, S. J. Interneuron and pyramidal cell interplay during in vitro seizure-like events. *J. Neurophysiol.* **95,** 3948–54 (2006).

119. Tuckwell, H. C. *Introduction to theoretical neurobiology - volume 1*. *Neurobiology* (1988). doi:10.2277/052101932X

120. Corticonics - Cambridge University Press. at <http://www.cambridge.org/catalogue/catalogue.asp?isbn=0521376173>

121. Hopfield, J. J. & Herz, a V. Rapid local synchronization of action potentials: toward computation with coupled integrate-and-fire neurons. *Proc. Natl. Acad. Sci. U. S. A.* **92,** 6655–6662 (1995).

122. Hansel, D., Mato, G. & Meunier, C. Synchrony in excitatory neural networks. *Neural Comput.* **7,** 307–337 (1995).

123. Campbell, S. R., Wang, D. L. & Jayaprakash, C. Synchrony and desynchrony in integrate-and-fire oscillators. *Neural Comput.* **11,** 1595–619 (1999).

124. Braun, H. a *et al.* Noise-induced precursors of tonic-to-bursting transitions in hypothalamic neurons and in a conductance-based model. *Chaos* **21,** 047509 (2011).

125. Brunel, N. Dynamics of sparsely connected networks of excitatory and

inhibitory spiking neurons. *J. Comput. Neurosci.* **8,** 183 – 208 (2000).

126. Tsodyks, M., Uziel, a & Markram, H. Synchrony generation in recurrent networks with frequency-dependent synapses. *J. Neurosci.* **20,** RC50 (2000).

127. Karnatak, R., Ansmann, G., Feudel, U. & Lehnertz, K. Route to extreme events in excitable systems. *Phys. Rev. E* **90,** 022917 (2014).

128. Sporns, O., Tononi, G. & Edelman, G. M. Theoretical neuroanatomy: relating anatomical and functional connectivity in graphs and cortical connection matrices. *Cereb. Cortex* **10,** 127–141 (2000).

129. Bressler, S. L. Large-scale cortical networks and cognition. *Brain Res. Rev.* **20,** 288–304 (1995).

130. He, Y., Chen, Z. J. & Evans, A. C. Small-world anatomical networks in the human brain revealed by cortical thickness from MRI. *Cereb. Cortex* **17,** 2407–2419 (2007).

131. Roxin, A., Riecke, H. & Solla, S. a. Self-sustained activity in a small-world network of excitable neurons. *Phys. Rev. Lett.* **92,** 198101–1 (2004).

132. Wu, J. Y., Guan, L. & Tsau, Y. Propagating activation during oscillations and evoked responses in neocortical slices. *J. Neurosci.* **19,** 5005–5015 (1999).

133. Delaney, K. R. *et al.* Waves and stimulus-modulated dynamics in an oscillating olfactory network. *Proc. Natl. Acad. Sci. U. S. A.* **91,** 669–673 (1994).

134. Wilson, H. R., Blake, R. & Lee, S. H. Dynamics of travelling waves in visual perception. *Nature* **412,** 907–910 (2001).

135. Rubino, D., Robbins, K. a & Hatsopoulos, N. G. Propagating waves mediate information transfer in the motor cortex. *Nat. Neurosci.* **9,** 1549–1557 (2006).

136. Hansel, D. & Sompolinsky, H. Synchronization and computation in a chaotic neural network. *Physical Review Letters* **68,** 718–721 (1992).

137. Feldman, D. E. The Spike-Timing Dependence of Plasticity. *Neuron* **75,** 556–571 (2012).

138. Josselyn, S. a., Köhler, S. & Frankland, P. W. Finding the engram. *Nat. Rev. Neurosci.* **16,** 521–534 (2015).

139. Aton, S. J., Suresh, A., Broussard, C. & Frank, M. G. Sleep promotes cortical response potentiation following visual experience. *Sleep* **37,** 1163–70 (2014).

140. Aton, S. J. *et al.* Visual experience and subsequent sleep induce sequential plastic changes in putative inhibitory and excitatory cortical neurons. *Proc. Natl. Acad. Sci. U. S. A.* **110,** 3101–6 (2013).

141. Vecsey, C. G. *et al.* Sleep deprivation impairs cAMP signalling in the hippocampus. *Nature* **461,** 1122–5 (2009).

142. Feldt, S., Waddell, J., Hetrick, V., Berke, J. & Å»ochowski, M. Functional clustering algorithm for the analysis of dynamic network data. *Phys. Rev. E* **79,** 1–20 (2009).